NJC

Accepted Manuscript

This is an *Accepted Manuscript*, which has been through the Royal Society of Chemistry peer review process and has been accepted for publication.

Accepted Manuscripts are published online shortly after acceptance, before technical editing, formatting and proof reading. Using this free service, authors can make their results available to the community, in citable form, before we publish the edited article. We will replace this *Accepted Manuscript* with the edited and formatted *Advance Article* as soon as it is available.

You can find more information about *Accepted Manuscripts* in the Information for Authors.

Please note that technical editing may introduce minor changes to the text and/or graphics, which may alter content. The journal's standard Terms & Conditions and the Ethical guidelines still apply. In no event shall the Royal Society of Chemistry be held responsible for any errors or omissions in this *Accepted Manuscript* or any consequences arising from the use of any information it contains.

ROYAL SOCIETY OF CHEMISTRY

www.rsc.org/njc

Nickel(II) dithiocarbamate complexes containing pyrrole moiety for sensing of anions and synthesis of nickel sulfide and nickel oxide nanoparticles

Ethiraj Sathiyaraj, Govindasamy Gurumoorthy and SubbiahThirumaran*

Department of Chemistry, Annamalai University, Annamalainagar-608 002.

Abstract

New homoleptic complexes bis(N-(pyrrol-2-ylmethyl)-N-butyldithiocarbamato-S,S′)nickel(II) (**1**), bis(N-(pyrrol-2-ylmethyl)-N-furfuryldithiocarbamato-S,S′)nickel(II) (**2**) and bis(N-(pyrrol-2-ylmethyl)-N-cyclopropyldithiocarbamato-S,S′)nickel(II) (**3**) and heteroleptic complexes (N-(pyrrol-2-ylmethyl)-N-butyldithiocarbamato-S,S′)(thiocyanato-N)triphenylphosphine)nickel(II) (**4**), (N-(pyrrol-2-ylmethyl)-N-furfuryldithiocarbamato-S,S′)(thiocyanato-N)(triphenylphosphine)nickel(II) (**5**) and (N-(pyrrol-2-ylmethyl)-N-cyclopropyldithiocarbamato-S,S′)(thiocyanato-N)(triphenylphosphine)nickel(II) (**6**) have been prepared and characterized by elemental analysis, IR, ^{1}H, ^{13}C NMR, HSQC, HMBC and UV-Vis absorption spectra. For the heteroleptic complexes, the thiocyanide ν_{C-N} values were shifted to higher wavenumbers and NCS_2 carbon signals were shifted to downfield compared to that of homoleptic complexes, suggesting increased strength of the thioureide bond due to the presence of π-accepting phosphine. Electronic spectral studies suggest square-planar geometry for the complexes. Complex **5** was also characterized by X-ray diffraction techniques and present a distorted NiS_2PN square planar configuration around the Ni atom. Rare C-H···Ni intramolecular short contact interactions were observed in the complex **5**. The ability of representative complexes **1** and **2** to sense of anions (F^-, Cl^-, $Br^-$and I^-) was examined by UV-Vis absorption spectra and cyclic voltametric titration studies. This studies show that both the complexes prefer

to bind with the I⁻. Complex **2** has been used as a single source precursor for the preparation of nickel sulfide and nickel oxide nanoparticles. The as-prepared nickel sulfide nanoparticles have been characterized by PXRD, SEM, EDAX, TEM, HRTEM, UV-Vis and Photoluminescence spectroscopy. X-ray diffraction analysis exhibited the presence of three phases (Cubic-NiS_2, Cubic-Ni_3S_4 and Rhombohedral-Ni_3S_2). TEM images of nickel oxide revealed that the particles are spherical shape with diameter ~30 nm.

Keywords: Nickel(II) dithiocarbamate; anagostic interaction; nickel sulfide , nickel oxide

1. INTRODUCTION

Transition metal dithiocarbamate complexes have been widely studied[1]. Because of their structural diversity[2], magnetic, electrochemical, thermal and conducting properties, potential applications as sensitizers in solar schemes, single source precursors for the preparation of metal sulfide nanoparticles[3] biology, agriculture and as antioxidant[4]. Optical and electrochemical properties of transition metal dithiocarbamate complexes favor the creation of anion sensors[5]. As a consequence of the many pivotal roles played by anions in medical, chemical, biological and environmental process stimulated the construction of molecular host system capable of complexing anionic guests. Here in we synthesized pyrrole based nickel dithiocarbamate complexes which are designed to coordinate anions via their pyrrole NH groups, precluding direct metal in coordination to the deprotonated pyrrole nitrogen atom. Transition metal chalcogenids as important semiconductor material, have attracted widely attention because of their wonderful physical and chemical properties and broad application in many fields[6-8]. Nickel sulfides can from various compositions such as NiS, $Ni_{3+x}S_2$, Ni_3S_2, Ni_7S_6, Ni_9S_8, Ni_3S_4, NiS_2[9-13]. Nickel sulfides posses electronic[14], electrical magnetic[15] and optical properties[16] and can be used

in various fields such as cathode materials in rechargeable lithium batteries,[17] catalysts for hydride nitrogen and hydro desulfurization[18-19] and IR detectors[20]. Nickel dithiocarbamate complexes have been used as single source precursors for synthesis of nickel sulfide nanoparticles are often influenced by the precursor[21-26]. Here, we reported synthesis and characterization of Nickel(II) dithiocarbamate complexes containing pyrrole moiety and their use for the sensing of anions and synthesis of nickel sulfide and nickel oxide nanoparticles. In addition, X-ray structure of complex **5** is also reported.

2. Experimental

Materials

All chemicals were purchased from commercial sources and used without further purification.

Physical measurements

The melting points were determined in open capillaries and are uncorrected. Elemental analysis was performed by (varioMICRO V2.2.O). IR spectra were recorded on a SHIMADZU FT-IR and thermo scientific NICOLET iS5 spectrophotometer (range 4000–400 cm^{-1}) as KBr pellets. The NMR spectra were recorded on Bruker 400/100 spectrometers at room temperature using TMS as internal reference. UV–vis and fluorescence spectra were recorded on a SHIMADZU UV-1650 PC and Perkin Elmer L555 spectrofluorimeter, respectively. Cyclic voltammograms were recorded on a CHI604C Electrochemical Analyser. The working electrode was platinum. The counter electrode was a platinum wire, and reference electrode was Ag/AgCl. Pure dichloromethane was used as the solvent and tetrabutylammonium fluoroborate (0.10 M) as the supporting electrolyte. The concentration of host and guest anions (F^-, Cl^-, Br^- and I^-) as their

tetrabutylammonium salts are 0.5×10^{-4} M and 2.5×10^{-4} M, respectively. The scan rate was 100 mV s^{-1}. All the measurements were recorded at room temperature (27°C) in an oxygen-free atmosphere, provided by bubbling purified nitrogen through the solution. TEM was performed using a Hitachi (H-7500) an operating voltage of 120 kV is equiped with CCD Camera. HRTEM images were recorded using a TECNAI T20 G2 make- FEI, Netherland KeV-200KeV LaB6 filament. Fluorescence spectra were recorded on a Perkin Elmer L555 spectrofluorimeter. Field Emission Scanning Electron Microscopy (FESEM, Carl Zeiss Supra 55) fitted with an energy dispersive X-ray spectrometer (EDAX) was used to characterize the morphologies and elemental analysis of the samples. The wide-angle X-ray diffraction (XRD) was recorded using Seifert Jhod Dye Flex 2002 diffractometer with CuK_α radiation (λ = 1.54178Å).

X-ray crystallography

Single crystals suitable for X-ray diffraction measurements were obtained by the slow evaporation of complex **5** in acetonitrile/methanol at room temperature. A purple-red colour crystals obtained was sorted using polarizing microscope. Crystals having good morphology were chosen for three-dimensional intensity data collection. This measurements were made on a bruker SMART APEXII area-detector diffractometer using graphite monochromated Mo$K\alpha$ radiation (λ = 0.71073) at ambient temperature. The structure was solved by SHELXS-97[27] and refined by full matrix least-squares method in SHELXL-97 [27]. All the non-hydrogen atoms were refined anisotropically and the hydrogen atoms were refined isotropically. Details of the crystal data and structure refinement parameters for **5** was summarized in **Table** 1 Crystallographic data for the structure reported in this paper have been deposited with the Cambridge Crystallographic Data Centre as supplementary publication No. CCDC-1037963. Copies of the data can be

obtained free of charge from the CCDC, 12 Union Road, Cambridge CB1 1EZ, UK (Tel: (+44) 1223-336-408; Fax: (+44) 1223-336-003; E-mail: deposit@ccdc.cam.ac.uk).

Table 1 .Crystal data, data collection and refinement parameters for complex 5

Empirical formula	C_{30} H_{26} N_3 Ni O P S_3
FW	630.40
Crystal dimensions (mm)	0.30 × 0.25 × 0.20
Crystal system	Monoclinic
Space group	P 21/n
a/Å	9.9973(2)
b/Å	12.1216(2)
c/Å	13.5814(3)
α/°	96.2470(10)
β/°	105.0470(10)
γ/°	108.5290(10)
V/Å^3	1473.76(5)
Z	2
Dc/g cm^{-3}	1.421
μ/cm^{-1}	0.954
F(000)	652
λ/Å	MoK$_\alpha$ (0.71073)
θ Range/°	1.59-26.48
Index ranges	-12≤ h ≤ 12, -15 ≤ k ≤ 15, -17≤ l ≤ 17
Reflections collected	22061
Observed reflections I > 2σ(I)	5099
Weighting scheme	Calc.w=1/[s^2(Fo^2)+(0.0477P)^2+0.7371P] where P=(Fo^2+2Fc^2)/3
Number of parameters refined	352
R[F^2 > 2σ(F^2)], wR(F^2)	0.0315, 0.0827
GOF	0.957

Theoretical studies

All calculations were performed with **GAUSSIAN09** program package[28] with the aid of the GaussView visualization program.

Preparations

Pyrrole based amines

Pyrrole-2-carboxyaldehyde (5.1 mmol) and amine (4.6 mmol) (butylamine, furfurylamine, cyclopropylamine) were dissolved in methanol (30 mL) and the solution was stirred for 2 h at room temperature. The solvent was removed by evaporation. The resulting colourless oil was dissolved in methanol-dichloromethane solvent mixture (1:1, 20 mL) and sodium borohydride (13.8 mmol) was added slowly at 5°C and stirred for 2 h before removal ice both. The reaction mixture was stirred at room temperature for 20 h. After evaporation of the solvent, the resulting viscous liquid was washed with water and dichloromethane was added in order to extract the product. Evaporation of the organic layer gave pyrrole based amines (**1-3**) as pale yellow oil.

Complexes (1-3)

Pyrrole based amine (4.0 mmol) in methanol was mixed with carbon disulphide (4.0 mmol) under ice cold condition. To the resultant yellow dithiocarbamic acid solution, aqueous solution of $NiCl_2 \cdot 6H_2O$ (2.0 mmol) was added with constant stirring. The solid which precipitated was washed several times with cold water and then dried.

Complexes (4-6)

A mixture of complex (**4-6)** (1.0 mmol, 0.624 g), PPh_3 (2.0 mmol, 0.524 g), $NiCl_2 \cdot 6H_2O$ (1.0 mmol, 0.237 g) and NH_4SCN (2.0 mmol, 0.152 g) was refluxed for 3 h in acetonitrile-methanol solvent mixture (1:1, 50 mL). The purple-red solution obtained was filtered and left for evaporation. After 2 days, a purple-red solid separated out which was recrystallized from dichloromethane.

Characterization data

1. Colour: olive green; Yield 74%, mp 149-151 °C. IR (KBr, cm^{-1}): ν = 3414 (ν_{N-H}); 1504 (ν_{C-N}); 1027 (ν_{C-S}). UV-Vis ($CHCl_3$, nm): λ = 627, 479, 386, 326, 253. ^{1}H NMR (400 MHz, $CDCl_3$, ppm): δ = 4.71 (s, 4H, NC***H***$_2$ (pyrrole)); 3.49 (t, 4H, N–C***H***$_2$–CH_2–CH_2–CH_3); 1.56 (m, 2H, N–CH_2–C***H***$_2$–CH_2–CH_3); 1.29 (m, 2H, N–CH_2–CH_2–C***H***$_2$–CH_3); 0.91 (t, 3H, N–CH_2–CH_2–CH_2–C***H***$_3$), 6.10-6.11 (d, 2H, ***H***-3 (pyrrole)); 6.16 (s, 2H, ***H***-4 (pyrrole)); 6.81 (s, 2H, ***H***-5 (pyrrole)); 8.83 (s, 2H, pyrrole N***H***); ^{13}C NMR (100 MHz, $CDCl_3$, ppm): δ = 13.7 (N–CH_2–CH_2–CH_2–***C***H_3), 19.9 (N–CH_2–CH_2–***C***H_2–CH_3), 28.8 (N–CH_2–***C***H_2–CH_2–CH_3), 45.4 (N–***C***H_2–CH_2–CH_2–CH_3), 48.7 (N***C***H_2 (pyrrole)), 108.1, 109.8, 119.6, 124.5 (pyrrole ring carbons), 206.3 (N***C***S_2). Anal. Calcd. for Chemical Formula: $C_{19}H_{26}N_4NiS_4$ (%): Elemental Analysis: C, 45.88; H, 5.27; N, 11.26. Found: C, 45.74; H, 5.21; N 11.19.

2. Colour: olive green; yield 68%, mp 164-166 °C. IR (KBr, cm^{-1}): ν =3399 (ν_{NH}); 1497 (ν_{C-N}); 1018 (ν_{C-S}). UV-Vis ($CHCl_3$, nm): λ = 629, 488, 389, 328, 254, 231. ^{1}H NMR (400 MHz, $CDCl_3$, ppm): δ = 4.67 (s, 4H, NC***H***$_2$ (pyrrole)); 4.71 (s, 4H, NC***H***$_2$ (furyl)); 6.14 (s, 2H, ***H***-3 (pyrrole)); 6.21 (s, 2H, ***H***-4 (pyrrole)); 6.83 (s, 2H, ***H***-5 (pyrrole)); 8.79 (s, 2H, pyrrole N***H***); 6.38 (s, 2H, ***H***-3 (furyl); ***H***-4 (furyl)); 7.43 (d, 2H, ***H***-5 (furyl)).^{13}C NMR (100 MHz, $CDCl_3$, ppm): δ =43.6 (N***C***H_2 (pyrrole)); 44.7 (N***C***H_2 (furyl)); 110.8-110.9 (***C***-3 Carbon overlapping With ***C***-4); 143.1 (***C***-2) (furyl ring carbons); 147.4 (***C***-5) (furyl ring carbons); 44.7 (N***C***H_2 (furyl)); 108.2, 110.3, 119.8, 123.9 (pyrrole ring carbons); 207.8 (N***C***S_2). Anal. Calcd. for Chemical Formula: $C_{22}H_{22}N_4NiO_2S_4$ (%): Elemental Analysis: C, 47.07; H, 3.95; N, 9.98. Found: C, 46.86; H, 3.84; N 9.89.

3. Colour: olive green; Yield 69%, mp 163-166°C. IR (KBr, cm^{-1}): ν =3399 (ν_{NH}); 1476 (ν_{C-N}); 1030 (ν_{C-S}). UV-Vis ($CHCl_3$, nm): λ = 620, 453,404, 326,254, 235 .^{1}H NMR (400 MHz,

$CDCl_3$, ppm): δ =4.72 (s, 4H, NC***H***$_2$ (pyrrole)); 2.71 (s, 2H, Cy–C***H*** (^{c}Pr)); 0.91(t, 4H, Cy–C***H***$_2$ (^{c}Pr)); 6.10-6.11 (d, 2H, ***H***-3 (pyrrole)); 6.16 (s, 2H, ***H***-4(pyrrole)); 6.79 (s, 2H, ***H***-5(pyrrole)); 8.83 (s, 2H, pyrrole N***H***);^{13}C NMR (100 MHz, $CDCl_3$, ppm): δ =7.5 (Cy–C***H***$_2$ (^{c}Pr)); 32.1 (Cy–C***H*** (^{c}Pr)); 46.8 (N***C***H$_2$ (pyrrole)); 108.0, 109.3, 119.2, 125.4 (pyrrole ring carbons); 211.4 (NCS_2). Anal. Calcd. for Chemical Formula: $C_{18}H_{22}N_4NiS_4$ (%): Elemental Analysis: C, 44.91; H, 4.61; N, 11.64. Found: C, 44.79; H, 4.54; N 11.56.

4. Colour; purple-red solid; Yield 82%, mp 172-174 °C. IR (KBr, cm^{-1}): ν = 3415 (ν_{NH}); 2095 (NCS), 1527 (ν_{C-N}), 1029 (ν_{C-S}). UV-Vis ($CHCl_3$, nm): λ = 485, 330, 271, 262, 235. ^{1}H NMR (400 MHz, $CDCl_3$, ppm): δ = 0.84 (br s, 3H, N–CH_2–CH_2–CH_2–C***H***$_3$), 1.24, 1.25 (bd, 2H, N–CH_2–CH_2–C***H***$_2$–CH_3), 1.57, 1.59 (bd, 2H, N–CH_2–C***H***$_2$–CH_2–CH_3), 3.30, 3.47 (bd, 2H, N–C***H***$_2$–CH_2–CH_2–CH_3), 4.51, 4.67 (bd, 2H, NCH_2 (pyrrole)); 6.12, 6.13 (d, 4H, ***H***-3 overlapping with ***H***-4 (pyrrole)); 6.8 (s, 2H, ***H***-5 (pyrrole)); 8.79 (bd, S, 2H, pyrrole N***H***), 7.24-7.71 (phenyl ring protons). ^{13}C NMR (100 MHz, $CDCl_3$, ppm): δ = 13.6, 13.7 (N–CH_2–CH_2–CH_2–***C***H_3), 19.8, 20.0 (N–CH_2–CH_2–***C***H_2–CH_3), 28.8 (N–CH_2–***C***H_2–CH_2–CH_3), 44.5, 45.0 (N–***C***H_2–CH_2–CH_2–CH_3), 48.6 (N***C***H$_2$ (pyrrole)), 108.3, 110.3, 119.9, 123.7 (pyrrole ring carbons), 128.0–134.2 (phenyl ring carbons), 203.1 (N***C***S_2). Anal. Calcd. for Chemical Formula: $C_{29}H_{30}N_3NiPS_3$(%): Elemental Analysis: C, 57.44; H, 4.99; N, 6.93. Found (%): C, 57.37; H, 4.92; N, 6.87.

5. Colour; purple-red solid; yield 82 %, mp 164-166 °C. IR (KBr, cm^{-1}): ν =3428 (ν_{NH}); 2093 (NCS); 1514 (ν_{C-N}); 1018 (ν_{C-S}). UV-Vis ($CHCl_3$, nm): λ = 487, 333, 249, 225. ^{1}H NMR (400 MHz, $CDCl_3$, ppm): δ = 4.53-4.61 (bd, 4H, NCH_2 (pyrrole) (furyl)); 6.13, 6.17 (d, 2H, ***H***-3 overlapping with ***H***-4 (pyrrole)); 6.82 (s, 1H, ***H***-5 (pyrrole)); 8.75-8.79 (b, 1H, pyrrole N***H***); 6.29-6.36 (d, 2H, ***H***-3 and ***H***-4 (furyl)); 7.50–7.72 (16H, phenyl ring protons with ***H***-5 furyl).^{13}C NMR (100 MHz, $CDCl_3$, ppm): δ =43.7 (N***C***H$_2$ (pyrrole)); 44.7 (N***C***H$_2$ (furyl)); 108.5, 110.7,

120.0, 123.1 (pyrrole); 110.8, 111.3, 143.5, 146.7 (furyl ring carbons); 128.0-134.2(phenyl ring carbons); 204.7 (N***C***S_2). Anal. Calcd. for Chemical Formula: $C_{30}H_{26}N_3NiOPS_3$ (%): Elemental Analysis: C, 57.16; H, 4.16; N, 6.67. Found: C, 57.03; H, 4.08; N 6.43.

6. Colour; purple-red solid, yield 76%, mp 138-142°C. IR (KBr, cm^{-1}): ν = 3298 (ν_{NH}); 2095 (NCS), 1491 (ν_{C-N}); 1030 (ν_{C-S}). UV-Vis ($CHCl_3$, nm): λ = 481, 331, 252 .^{1}H NMR (400 MHz, $CDCl_3$, ppm): δ = 4.71, 4.65 (b, 4H, NC***H***$_2$ (pyrrole)); 2.61 (s, 2H, Cy-C***H*** (^{c}Pr)); 0.84 (b, 4H, Cy-C***H***$_2$(^{c}Pr)); 6.11 (d, 2H, H-3 overlapping with H-4 (pyrrole)); 6.79 (s, 1H, H-5 (pyrrole)); 8.88 (s, 1H, pyrrole N***H***); 7.27–7.71 (15H, phenyl ring protons); ^{13}C NMR (100 MHz, $CDCl_3$, ppm): δ =7.2-7.5 (Cy-***C***H_2(^{c}Pr)); 31.9 (Cy-***C***H(^{c}Pr)); 46.8 (N***C***H_2 (pyrrole)); 108.0-108.3, 109.2-109.7, 119.4, 124.4 (pyrrole ring carbons); 128.1-134.2 (phenyl ring carbons); 208.1 (N***C***S_2). Anal. Calcd. for Chemical Formula: $C_{28}H_{26}N_3NiPS_3$ (%): Elemental Analysis: C, 56.96; H, 4.44; N, 7.12. Found: C, 56.88; H, 4.36; N 6.97.

Preparation of nickel sulfide nanoparticles

0.5 g of complex **2** was dissolved in 30 mL of ethylenediamine in a flask and then heated to reflux and maintained at this temperature for 15 min. The precipitate obtained was filtered off and washed with methanol.

Preparation of nickel oxide nanoparticles

The NiO nanoparticle was synthesized by thermal decomposition of complex **2**. 1 g of complex **2** was heated in muffle-furnace at 600°C for 30 min in the presence air atmosphere. The final residue analysed to nickel oxide.

3. Results and discussion

Spectroscopy

In the infrared spectra of the metal complexes, two diagnostic bands are important. First is the band due to ν_{C-N} thioureide which is observed in the region 1450-1550 cm^{-1} indicating the partial double bond character. In the present study, homoleptic and heteroleptic complexes show $C\overset{\cdots\cdots}{=\!=}N$ bands in the region 1491-1527 cm^{-1}.[29-30] The higher vibrational frequency observed for the heteroleptic complexes compared to parent homoleptic complexes indicate a partial double character of the ν_{C-N} arising mesomeric drift of electron density from the dithiocarbamate moiety towards the nickel(II) centre. The second band which observed in the region 1018-1030 cm^{-1} without any splitting corresponds to ν_{C-S} vibration and indicates bidentate coordination mode of the dithiocarbamate moiety through the two sulfur donor atom[31]. The bands which appear in the region 3298-3428 cm^{-1} is assigned to N-H stretching frequency of pyrrole group. A band observed at higher wave number around 2093 cm^{-1} for all heteroleptic complexes are attributed to the N-coordinated thiocyanate anion.

Electronic spectra of homoleptic complexes **1-3** show weak bands around 620 and 480 nm. These two bands correspond to $d_{xy} \rightarrow d_{x^2-y^2}$ and $d_{z^2} \rightarrow d_{x^2-y^2}$ transitions, respectively. Heteroleptic complexes **4-6** show a band at 480 nm which can be attributed to the d-d transitions. Comparison of the information already available on similar compounds of this type leads to the conclusion that the coordination around the metal centres is probably square planar. The bands observed below 350 nm arise from intraligand π-π* charge transfer transition mainly associated with N-C=S and S-C=S groups[32]. The intense band appears around 400 nm is attributed to either metal→ ligand or ligand→metal charge transfer transition.

The methylene protons attached to pyrrole group of all the complexes appear around 4.7 ppm. The methylene protons adjacent to nitrogen atom of butyl and furfuryl of dithiocarbamate ligand are observed in between 3.3-4.7 ppm. A broad signal observed around 0.85 ppm for complexes **3** and **6** are assigned to methyne groups. The other alkyl protons appear in the region 0.84 to 1.58 ppm. The deshielding of the methylene and methyne protons adjacent to nitrogen atom is attributed to the release of electrons of nitrogen forcing a high electron density towards the sulfur (or metal) via thioureide π- system. A signal around 8.8 ppm is assigned to the N-H proton of pyrrole group. The signals observed in the downfield region 6.1 to 7.7 ppm for all the complexes are due to the aromatic protons.

In the ^{1}H NMR spectrum of **2**, there are two sharp signals at 4.67 and 4.71 ppm, corresponding to each has four proton integral values. This should be due to the methylene protons of furfuryl and pyrrole methylene protons. There are five signals appeared in aromatic region at 6.13, 6.21, 6.39, 6.83 and 7.43 ppm. The pyrrole ring proton signals are observed at 6.13, 6.21 and 6.83 ppm, each one corresponding to two protons. These are due to H-3, H-4 and H-5, respectively. The furyl ring proton signals are appeared at 6.39 and 7.43 ppm. A signal at 6.39 ppm corresponding to four proton integral values is due to H-3 overlapping with H-4 furyl ring protons. Another signal with two proton integral at 7.43 ppm is assigned to H-5 proton of furyl ring[33].

Clearly resolved ^{13}C NMR signals were obtained for all the distinct carbon atoms present in the compounds. The most of the important ^{13}C NMR signals of the S_2CN carbon appear in the expected region (above 202 ppm) for normal oxidation state transition metal dithiocarbamate complexes.[34] These signals are observed in the region 203 to 212 ppm for all the complexes. In the case heteroleptic complexes (**4-6**) (203.1-208.1 ppm), an upfield shift is observed compared

with that found in homoleptic complexes (**1-3**) (206.3-211.4 ppm). The triphenylphosphine in heteroleptic complexes increase the mesomeric drift of electron density from the dithiocarbamate moiety toward the metal atom. This increases the C-N partial double bond character, and as a result displacement of the electron density from the nitrogen atom of the dithiocarbamate group.[35] This explains the shielding of NCS_2 carbon of heteroleptic complexes.[36]

To confirm the assignments made through 1D NMR and to assign two methylene proton signals of pyrrole and furfuryl groups which appear at 4.66 and 4.71 ppm. 2D NMR namely HSQC and HMBC spectra were recorded for complex **2** and are shown in **Figs. 1**and **2**. Correlation for protons in dithiocarbamate are given in **Tables S1** and **S2**.

^{1}H-^{13}C connectivity in complex **2** can be readily established using its HSQC spectrum and their correlations are given in **Table S1.** The pyrrole ring proton signals at 6.13, 6.21 and 6.83 ppm are also cross peak with C-4, C-3 and C-5, respectively. The furyl ring proton signal at 6.38 shows cross peak with C-3 and C-4 carbons. Proton signal at 7.43 ppm exhibits cross peak with C-5 carbon of furyl ring. HSQC spectrum of complex **2** confirms the assignment of C-3, C-4 and C-5 carbons of pyrrole and furyl rings.

Table:S1 Correlations in the HSQC spectrum of complex

^{13}C Chemical shifts (δ, ppm)	Correlation in the **HSQC** spectrum
43.6 (CH_2- pyrrole)	4.67 (furyl)
44.7 (CH_2-furyl)	4.71(pyrrole)
123.9 (C-2) pyrrole	-
110.3(C-3) pyrrole	6.21
108.1(C-4) pyrrole	6.13
119.8 (C-5) pyrrole	6.83
147.4(C-2) furyl	-
143.1(C-5) furyl	7.43
110.8 (C-3), 110.9 (C-4) furyl	6.38

The ^{13}C signals for carbon without hydrogens are assigned based on the observed correlations in the HMBC spectrum. The observed HMBC correlations are given in Table **T2**

Table: S2 Correlations in the HMBC spectrum of complex 2

^{13}C Chemical shifts (δ, ppm)	Correlation in the **HMBC** spectrum
43.6 (CH_2-pyrrole)	4.71 (H-1)
44.7 (CH_2-furyl)	4.67 (H-1)
123.9 (C-2) pyrrole	6.83(H-5), 6.21(H-4), 4.71(furyl)
119.8 (C-5) pyrrole	-
110.3(C-3) pyrrole	-
108.1(C-4) pyrrole	-
147.4(C-2) furyl	7.43 (H-5), 6.38 (H-4), 4.66 (pyrrole)
143.1(C-5) furyl	-
110.8, 110.9 (C-3) (C-4) furyl	-

In the HMBC spectrum, the weak signal appeared at 147.4 ppm shows correlation with H–4, H–5 of furyl protons and methylene protons (H-1) of pyrrole. Other weak signal at 123.9 ppm shows correlation with H–4, H–5 of pyrrole ring protons and methylene protons (H-1) of furfuryl group. The signals observed at 43.6 and 44.7 ppm exhibit correlation with methylene protons of furfuryl (4.71 ppm) and pyrrole (4.67 ppm) respectively. These correlations confirm the assignments of methylene carbons of pyrrole and furfuryl groups**.**

Single crystal X-ray analysis of complex 5

The ORTEP diagram of **5** is depicted in **Fig. 3**. Selected bond distances and angles are presented in **Table 2**. The Ni(II) is tetracoordinated by two sulfur atoms from a bidentate dithiocarbamate ligand, one nitrogen atom from thiocyanate and one phosphorus atom from triphenylphosphine. The geometry of this coordination polyhedron [NiS_2PN] is a distorted square planar. The

structure adopted by this complex is characterized by the τ_4 descriptor for four coordination suggested by yang *et.al*.[37]. The τ_4 values of this complex is 0.13; which indicates that the coordination geometry is a see saw (τ_4=0.64-0.07) structure. The dithiocarbamate ligand in complex **2** coordinate in an anisobidentate fashion [Ni-S2= 2.1829(6) and Ni-S3=2.2175(5) Å]. The Ni-S distances are asymmetric i.e, Ni-S bond *trans* to PPh_3 is longer than the other Ni-S bond. This is due to the more effective *trans* influence of PPh_3 over NCS^-. The S-C bond lengths [1.7093(19) and 1.7199(19) Å] also show the anisobidentate nature of the ligand. The both C-S distances are intermediate between single bond (1.81Å) and double bond (1.60Å) distances. Similarly, the C20-N2 bond length 1.305(2) Å is significantly shorter than a normal C-N bond distance (1.47Å) and longer than a C=N bond length (1.28 Å). These bond values clearly demonstrate the resonance phenomenon in NCS_2 moiety. The Ni-N distance is 1.8613(19), which is similar to that observed in similar complexes. The short Ni-P distance 2.2064(5) reveals a strong back bonding interaction between Ni and P in the complex.

In the crystal structure of **5**, neighboring molecules are linked by C-H···S contacts, thus generating the dimers (**Fig. S1**). The packing is further stabilized by additional C-H···π interaction between methylene and furyl ring (**Table 3** and **Fig. 4**) and intramolecular C-H···S interactions (**Fig. S2**). C-H···M interaction are of three types (i) hydrogen bond (ii) agostic and (iii) anagostic or preagostic[38-39]. Hydrogen bonds are 3-centre-4-electron intractions with an almost linear geometry. Agostic M···H-C interactions are usually referred to as 3-centre-2-electron interaction and characterized by relatively short M···H distances of ≈1.8-2.3Å and <C-H···M ≈ 90-140°. Such interactions are often found in d^6 complexes. Anagostic interactions are largely electrostatic in nature with M···H distance of ≈2.3-2.9 Å and <C-H···M =110-170°. Anagostic interactions occurring square planer d^8 system are believed to be involved in many

catalytic process.[40-41] In this complex, as a results of packing effects together with the steric and electronic restrictions of bulky ligands and the d^8 electronic configuration, one of the phenyl rings in the PPh_3 is tilted more towards the central atom facilitating rare intramolecular C-H···Ni anagostic interaction via an ortho phenyl proton of PPh_3 (H···Ni distance 2.784 Å and C-H···Ni angle 120.13°) (**Fig. 5**). The hydrogen atom is in an approximately axial position to the metal.

Table 2. Selected bond lengths (Å) and bond angles (°) of complex **5.**

Bond length		Bond angle	
C1-N1	1.146(3)	N1-C1-S1	178.0(2)
C1-S1	1.618(2)	N2-C20-S3	125.43(14)
C20-N2	1.305(2)	N2-C20-S2	125.79(14)
C20-S3	1.7093(19)	S3-C20-S2	108.75(11)
C20-S2	1.7199(19)	C1-N1-Ni1	172.0(2)
N1-Ni1	1.8613(19)	C20-N2-C21	121.51(17)
P1-Ni1	2.2064(5)	C26-N2-C21	117.18(17)
S2-Ni1	2.1829(6)	C27-N3-C30	106.4(3)
S3-Ni1	2.2175(5)	C20-S2-Ni1	86.74(7)
		C20-S3-Ni1	85.89(7)
		N1-Ni1-S2	171.04(6)
		N1-Ni1-P1	95.58(6)
		S2-Ni1-P1	92.43(2)
		N1-Ni1-S3	93.19(6)
		S2-Ni1-S3	78.61(2)
		P1-Ni1-S3	170.68(2)

Table.3 Hydrogen bonding parameters for complex **5**

Interactions	**D─H**	**H···A**	**D···A**	**D─H···A**
C26─H26A···S1	0.97	2.912	3.770	148.00
C26─H26B···S3	0.97	2.915	3.878	171.76
C26─H26B···S3	0.97	2.693	3.064	103.20
C21─H21A···S2	0.971	2.611	3.089	110.55
C15─H15···Ni	0.930	2.784	3.348	120.13
C21─H21···π	0.971	2.697	3.410	130.72

In the crystal structure of complex **5**, neighboring molecules are linked by C-H···S contacts, thus generating the dimmers.

Theoretical calculations

The optimized structure of complex **5** was given in **Fig.** 6. The theoretical and experimental values for the selected bond length and bond angles are given in Table **2**. Theoretical bond length values are slightly greater than experimental values.

Table 4. Selected bond distances (Å), bond angle (°) by theoretical and X-ray calculations for complex **5**

Bond distance	Theoretical HF/LANL2DZ	XRD	Bond angle	Theoretical HF/LANL2DZ	XRD
C1-S1	1.674	1.618(2)	N1-C1-S1	178.86	178.0(2)
N1-C1	1.168	1.146(3)	N2-C20-S3	124.48	125.43(14)
Ni1-N1	1.898	1.861(9)	N2-C20-S2	122.98	125.79(14)
Ni1-S3	2.397	2.217(5)	S3-C20-S2	112.51	108.75(11)
Ni1-S2	2.379	2.182(6)	C1-N1-Ni1	174.82	172.0(2)
C20-S3	1.774	1.709(19)	N1-Ni1-P1	89.579	95.58(6)
C20-S2	1.793	1.719(19)	S2-Ni1-P1	97.443	92.43(2)
N2-C20	1.139	1.305(2)	N1-Ni1-S3	96.164	93.19(6)
			S2-Ni1-S3	76.810	78.61(2)

The asymmetry in Ni-S (Ni-S2= 2.1829(6) and Ni-S3= 2.2175(5)) distance appeared in experimental structure analysis due to the *trans* effect of PPh_3 is not observed in calculated values (Ni-S2=2.3792 and Ni-S3=2.3971 Å). The experimental (anagostic interaction) and theoretical bond distance of M···H are 2.784 and 3.175 Å respectively. These differences between experimental and theoretical values are due to the following reason; all of the calculated data are for the molecule in gas phase and these are no inter-and intramolecular interactions while the

experimental data are for the molecule in solid state and there are molecular interactions among them. The frontier molecular orbitals play an important role in the electric and optical properties, as well as in UV-Vis spectra and chemical reactions[42]. The frontier molecular orbital **5** is shown in Fig **S3**.

HOMO energy = -7.994 eV

LUMO energy=1.887 eV

Energy gap=9.881 eV

The smaller band gap energy increases the stability of the molecule.

Molecular electrostatic potential

Molecular electrostatic potential plot of complex **5** is shown in **Fig S4**. The MEP map of complex **5** shows that more negative charge delocalized on the sulfur atom of thiocyanate. This is supported by the S···H-C interaction in the solid state.

Anion binding studies

Recently the use of the pyrrole group in anion recognition has received considerable attention. Therefore, the anion binding properties of the nickel(II) complexes containing pyrrole moiety synthesized in this study are of the interest. These complexes bind to anions via their pyrrole NH groups [5]. Preliminary anion binding studies of complexes **1** and **2** were carried out**.**

UV-vis titration

The binding of fluoride, chloride, bromide and iodide anions with complexes **1** and **2** was studied initially by UV-Vis titration method. The titrations were carried out in dichloromethane at $2x10^{-5}$ M concentration of host and increasing concentrations of $2x10^{-5}$ M (0-1 equivalents) solution of the guest anions (F^-, Cl^-, Br^- and I^-) as their tetrabutylammonium salts. Shifts (principally in absorbance) in the spectra were observed upon addition of anions. As shown in **Figs. 7** and **8**, the

complexes **1** and **2** ($2x10^{-5}$ M) show the absorption peak λ_{max} at 330 nm and 246 nm. Significantly, the absorption peak at 330 nm decreases where as the absorption peaks at 246 nm increases with the addition of iodide ion in complex **1**, accompanying the formation of an isobestic point at 280 nm **(Fig. 8)**. In other cases, absorption maxima of both bands decreases with the addition of anions.

Electrochemical properties of the receptors.

Cyclic voltammetric investigations of the Ni(II) complexes displayed a peak at around -1.2 V which corresponds to the normally observed and well documented Ni(II)/Ni(I) reduction (one electron addition). The addition of F^-, Cl^-, $Br^-$and I^- anions to electrochemical solutions of the complexes **1** and **2** resulted in significant shift in the Ni(II)/Ni(I) reduction potential (**Table 5 and Fig. 9**). **Table 5** shows that the anion induced magnitudes of anodic shift in the respect of Ni(II)/Ni(I) reduction potential. **Table 5** suggests that both the complexes show a preferential binding interaction with the I^-. For a given anion, the shift in the reduction potential of **1** and **2** is different. This reveals that the shift in reduction potential is affected by N-bound organic moiety in the dithiocarbamate ligand.

Table 5. Electrochemical anion recognition data[a]

S.No	Anions	Complex-**1** $\Delta E_{1/2}$(V)	Complex-**2** $\Delta E_{1/2}$(V)
1	TBA Fluoride	-0.037	-0.051
2	TBA Chloride	-0.311	-[b]
3	TBA Bromide	-0.265	-0.442
4	TBA Iodide	-0.564	-0.898

[a]Shift of Ni(II)/Ni(I) reduction potential produced by the anions

[b] No significant change in the reduction potential

Characterization of nickel sulfide nanoparticles

PXRD pattern of nickel sulfide nanoparticles is shown in figure. PXRD diffraction peaks could be indexed to NiS_2 cubic (JCPDS card no **89-7142**), Ni_3S_4 cubic (JCPDS card no **76-1813**) and Ni_3S_2 rhombohedral (JCPDS cards no **85-0775**) phases. In **Fig. 10**, the diffraction peaks of cubic NiS_2, cubic Ni_3S_4 and rhombohedral Ni_3S_2 phases are indicated by *, + and **o** respectively.

The elemental composition of the as-formed nickel sulfide nanoparticles was studied by EDAX spectral analysis. EDAX spectrum of nickel sulfide is shown in **Fig.11**. This confirms that the nanoparticles are composed of Ni and S.

The SEM image of nickel sulfide is shown in **Figure 12**. This image reveals that the product is spherical in shape.

TEM and HRTEM image of as-synthesized nickel sulfide nanoparticles are shown in **Figs. 13 and 14**. TEM images show that nickel sulfide nanoparticles were predominantly spherical but some flake like particles **Fig.13 (a**) are also seen. Spherical and flake particles as highlighted in **Fig. 13(b)** and **13(c),** respectively. **Fig. 13**(d) shows the zoom of a selected flake particle. The diameter of the spherical particles is ~30 nm and the length and width of the flake shape particles are 100 and ~35 nm, respectively. The formation of spherical like morphology is confirmed by HRTEM. **Fig. 14(a-b**) clearly exhibit that the nanoparticles have spherical particles. The d-spacing calculated from the spherical nanoparticles was found to be 2.8 Å corresponding to the (111) for NiS_2 and (311) for Ni_3S_4 plane and also supports the XRD analysis (**Fig. 14(c**)). **Fig. 14(d)** shows that the SAED pattern confirms the formation of polycrystalline nature of nickel sulfide.

The optical property of nickel sulfide nanoparticles dispersed in pure ethanol were investigated with ambient temperature UV-Vis absorption spectroscopy (**Figure 15 (a)**). The UV-Vis absorption spectrum of nanoparticles displays an absorption peak located at 346 nm (3.6 eV). The absorption by comparing the absorption peak with bulk nickel sulfide (590 nm; 2.1 eV)[43] it can be seen that a blue shift onset of absorption peak is absorbed in as-prepared nickel sulfide nanoparticles. The phenomenon of blue shift of absorption peak has been ascribed to a decrease in particle size. It is well known that in case of semiconductor, the band gap between the valence and conduction band increases as the size of particle decreases in the nanosize range. This results in a shift in the absorption peak to a lower wavelength region.

Fig. 15(b) shows the photoluminescence spectrum of the obtained nickel sulfide nanoparticles (excitation at 450 nm) at room temperature. It is clear that a broad peak with λ_{max} at 368 nm is observed in the spectrum. This is shorter than the bulk nickel sulfide indicating that as-prepared nanoparticles obtain in this work is in the quantum size[44]. No sharp PL line is absorbed in the spectrum. This is attributed to impurity band excitons and their phonoreplicas[45].

TG and DTA plots of ethylenediamine capped nickel sulfide nanoparticles are shown in **Fig.16**. TG curve shows a single step decomposition. The mass loss is due to the decomposition of ethylenediamine. (eqn.1)

$$Ni_3S_4\ (en)_x \rightarrow Ni_3S_4 + x\ en \rightarrow 1$$

Infrared spectrum of nickel sulfide nanoparticles is shown in Fig. **S5**. the bands appeared at 2922 and 2827 cm^{-1} are due to the C-H symmetric and asymmetric stretching vibrations of methylene groups. The N-H stretching vibrations are observed at 3292 and 3165 cm^{-1} and deformation vibration is appeared at 1589 cm^{-1}. These confirm the presence of ethylenediamine in nickel sulfide. The absence of aromatic C-H and N-CS_2 stretching vibration in the FT-IR

spectrum of nickel sulfide indicates that there is no dithiocarbamate ligand present in nickel sulfide.

Characterization of Nickel oxide nanoparticles

Fig.17 shows XRD patterns of the residue. The three diffraction peak at angles observed at 2Θ = 37.18, 43.21 and 62.81 are due to (003), (012) and (014) planes, respectively. Which correspond to NiO (JCPDS 47-1049) (JCPDS, No 71-1179). The remaining small peaks at 2Θ =11.68, 12.54, 20.79 and 27.13 indicate the presence of trace amount of $NiSO_4$. Energy Dispersive X-ray Spectral Analysis (EDAX) supports the presence Ni, O and S **(Fig.18)**. NiO and $NiSO_4$ were obtained as a final residue in thermogravimetric analysis of nickel–dithiocarbamate complexes[46].

Fig.19 show the FESEM images of nickel oxide nanoparticles. TEM images (**Fig.20)** reveal that the particles are spherical shape with diameter in the range 15-40 nm.

UV–visible absorption spectrum of the nickel oxide, which are ultrasonically dispersed in absolute ethanol, are shown in **Fig. 21(a)**. The distinct peak at 333 nm (3.72 eV) is due to the first exciton absorption band. The large blue shift relative to the bulk NiO[47] indicates the existence of strong quantum confinement effect.

The PL spectrum of the nickel oxide nanoparticles using a 300 nm excitation is shown in **Fig. 21(b)**. A strong peak at 444 nm in PL spectrum is attributed to the trap states emission. Generally, it is known that the PL properties of particles are influenced by many factors, such as particle size, shape, crystal surface state etc. Defects normally act as sites for nonradiative recombination of electron hole pairs. In this case, the sharp and high intensity emission indicates

the higher crystallinty with low concentration defects of the as-prepared nickel oxide nanoparticles.

4. Conclusions

IR and ^{13}C NMR spectral studies reveal that the increase in strength of the thioureide bond in the complexes **4-6** compared to **1-3** is due to the presence of π-accepting triphenyl phosphine. X-ray structure of complex **5** showed increasing inter-and intramolecular interactions. Especially rare C-H···Ni interaction was observed in complex **5** involving one of the ortho hydrogen atoms of the phenyl rings of the triphenylphosphine. Complexes with this type of interaction (C-H…Ni) are important due to their possible involvement in the C-H bond activation in the organic synthesis. This study demonstrates that the spherical shape of nickel sulfide and nickel oxide nanoparticles can be prepared from nickel(II) dithiocarbamate complexes. Cyclic voltammetric studies indicates that the shift in reduction potential on the addition of anions is affected by the N-bound organic moiety of dithiocarbamte ligand.

Acknowledgements

Dr. S. Thirumaran is thankful to University Grants Commission (UGC), India (F. No. 42-341/2013 (SR)) for providing fund for this research study. We are thankful to SAIF, Indian Institute of Technology-Madras and SAIF, Panjab University, Chandigarh, India, for the single crystal X-ray structural analysis and for recording TEM images, respectively. The authors are thankful to Dr SP. Meenakshisundram, Professor&Head, Department of Chemistry, Annamalai University-India, for providing GAUSSIAN09 program. E. Sathiyaraj gratefully acknowledges the University Grants Commission (UGC), India, for the award of Basic Sciences Research (BSR)-Special Assistant Programme (SAP) Fellowship.

5. References

1. G. Hogarth, *Prog. Inorg. Chem.,* 2005, **53**, 71-561.

2. M.J. Cox and E.R.T. Tiekink, *Rev. Inorg. Chem.,* 1997, **17**, 1-23.

3. N. Srinivasan and S. Thirumaran, *Synthesis and Reactivity in Inorganic, Metal-Organic, and Nano-Metal Chemistry,* 2013, **43**, 1256–1263,

4. H. Pang, D. Chen, Q. C. Cui and Q. P. Dou, *Int. J. Mol. Med.,* 2007, **19**, 809–816.

5. P. D.Beer, A.G. Cheetham, M.G.B. Drew, O. Danny fox, E.J. Hayes and T D. Rolls, *Dalton trans.*, **2003**, 603-611.

6. K. Mitchell and J.A. Ibers, *Chem. Rev.,* 2002, **102**, 1929-1953.

7. D. Yu and Z. Bai, *Appl. Phys. Lett.,* 1998, **72**, 3458-3460.

8. S. Frank, P. Poncharal, Z.L. Wang and W.A. de Heer, *Science,* 1998, **280**, 1744-1746.

9. A. Olivas, J. Cruz-Reyes, V. Petranovskii, M. Avalos and S. Fuentes, *J.Vac. Sci. Technol., A, Vac. Surf. Films,* 1998**, 16**, 3515-3520.

10. R.D. Tilley and D.A. Jefferson, *J. Phys. Chem., B*, 2002**, 106**, 10895-10901.

11. G. Kullerud and R.A. Yund, *J. Petrol.* 1962, **3**, 126-175.

12. H. Seim, H. Fjellvag, F. Groenvold and S. Stoelen, *J. Solid State Chem.* 1996, **121**, 400.

13. S. Stolen, H. Fjellvag, F. Gronvold and H. Seim, *J. Chem. Thermodyn.* 1994, **26**, 987-1000.

14. J.H. Wang, Z. Cheng, J.L. Bredas and M.L. Liu, *J. Chem. Phys.* 2007, **127**, 8214705.

15. W. Wang, S.Y. Wang, Y.L. Gao, K.Y. Wang and M. Liu, *Mater. Sci. Eng. B-Solid State Mater. Adv. Technol.* 2006, **133**, 167–171.

16. R. Luo, X. Sun, L.F. Yan and W.M. Chen, *Chem. Lett*. 2004**, 33**, 830–831.

17. S.C. Han, K.W. Kim, H.J. Ahn, J.H. Ahn and J.Y. Lee, *J. Alloys Compd*. 2003, **361**, 247–251.

18. A. Olivas, J. Cruz-Reyes, M. Avalos, V. Petranovskii and S. Fuentes, *Mater. Lett.* 1999, **38**, 141–144.

19. A. Olivas, J. Cruz-Reyes, V. Petranovskii, M. Avalos and S. Fuentes, *J. Vac. Sci.Technol. A* 1998, **16**, 3515–3520.

20. F. Atay, S.K. Ose, V. Bilgin and I. Akyuz, *Turk. J. Phys.* 2003, **27**, 285–292.

21. K. Ramasamy, M. A. Malik, P. O'Brien and J. Raftery, *Dalton Trans.,* 2010, **39**, 1460–1463.

22. B. Arul Prakasam, M. Lahtinen, A. Peuronen, M. Muruganandham, E. Kolehmainen, E. Haapaniemi and M. Sillanpaa, *Polyhedron,* 2014, **81**, 588-596.

23. P. Valarmathi, S. Thirumaran, L. Sarmal and Rajni Kant, *Spectrochim. Acta A*, 2014, **129**, 285-292.

24. R. Chauhan, M. Trivedi, J. Singh, K.C. Molloy, G. Kociok-Kohn, U. P. Mulik, D. P. Amalnerkar and A. Kumar, *Inorg. Chim. Acta.,* 2014**, 415**, 69-74.

25. P. O'Brien and J. Waters, *Chem. Vap. Deposition*, 2006, **12**, 620-626.

26. B. Arul Prakasam, M. Lahtinen, A. Peuronen, M. Muruganandham, E. Kolehmainen, E. Haapaniemi and M. Sillanpaa, *Inorg.Chim.Acta*, (in press) http://dx.doi.org/10.1016/j.ica.2014.09

27. G. M. Sheldrick, *Acta Cryst A* , 2008, **64**, 112–122

28. M.J. Frisch, G.W. Trucks, H.B. Schlegel, G.E. Scuseria, M.A. Robb, J.R. Cheeseman, G. Scalmani, V. Barone, B. Mennucci, G.A. Petersson, H. Nakatsuji, M. Caricato, X. Li, H.P. Hratchian, A.F. Izmaylov, J. Bloino, G. Zheng, J.L. Sonnenberg, M. Hada, M. Ehara, K. Toyota, R. Fukuda, J. Hasegawa, M. Ishida, T. Nakajima, Y. Honda, O. Kitao, H. Nakai, T. Vreven, J.A. Montgomery Jr., J.E. Peralta, F. Ogliaro, M. Bearpark, J.J. Heyd, E. Brothers, K.N. Kudin, V.N.

Staroverov, R. Kobayashi, J. Normand, K. Raghavachari, A. Rendell, J.C. Burant, S.S. Iyengar, J. Tomasi, M. Cossi, N. Rega, J.M. Millam, M. Klene, J.E. Knox, J.B. Cross, V. Bakken, C. Adamo, J. Jaramillo, R. Gomperts, R.E. Stratmann, O. Yazyev, A.J. Austin, R. Cammi, C. Pomelli, J.W. Ochterski, R.L. Martin, K. Morokuma, V.G. Zakrzewski, G.A. Voth, P. Salvador, J.J. Dannenberg, S. Dapprich, A.D. Daniels, Ö. Farkas, J.B. Foresman, J.V. Ortiz, J. Cioslowski, D.J. Fox, Gaussian Inc., Wallingford CT, Gaussian 09, Revision D.01, **2009**.

29. F. Bonati, R. Ugo, *J. Organomet. Chem.* 1967, **110**, 257.

30. R. Thiruneelakandan, K. Ramalingam, G. Bocelli, and L. Righi, *Z. Anorg. Allg. Chem.,* 2005, **631**,187-19

31. G. Hogarth, Ebony-Jewel C.-R.C.R. Rainford-Brent, Shariff E. Kabir, Idris Richards, James D.E.T. Wilton-Ely, Qi Zhang, *Inorg.Chim.Acta*, 2009, **362**, 2020–2026.

32. R. Pastorek, J. Kamenick, Z. Travnecik, J. Husaret, N. Dutty Polyhedron, 1999, **18,** 2879-2883.

33. R.M. Silver stein, F.X. Webster, Spectrometric identification of organic compounds, sixth edition, page 210, **2006**

34. H.C.M. Van Gael, J.W. Diesveld, F.W. Pijpans and J.G.M. Van der Lin don, *Inorg. Chem.,* 1979, **18**, 3251-3260.

35. N.Srinivasan, V.Sathyaselvabala, K. Kuppulekshmy, P. Valarmathi and S. Thirumaran, *Monatsh.Chem*.2009, **140**, 1431-1436.

36. P. Jamuna Rani, S. Thirumaran and Samuele Ciattini, *Phosphorus, Sulfur, and Silicon*, 2013, **188**, 778–789.

37. L.Yang, D.R. Powell and R.P. Houser, *Dalton Trans.* 2007, 955-964.

38. L. Brammer, *Dalton Trans*.2003, 3145 -3157.

39. J. C. Lewis, J. Wu, R. G. Bergman and J. A. Ellman, *Organometallics*. 2005, **24**, 5737-5746.

40. H. V. Huynh, L. R. Wong and P. S. Ng, *Organometallics,* 2008, **27**, 2231-2237.

41. Y. Zhang, J. C. Lewis, R. Bergman, J. A. Ellman and E. Oldfield, *Organometallics,* 2008, **25**, 2231.

42. I. Fleming, Frontier Orbitals and Organic Chemical Reactions, *John Wiley & Sons*, New York, 1976.

43. M.Salavati-Niasari, F.Davar and M.Mazaheri, *Mat.Res.Bull.,* 2009, **44**, 2246-2251.

44. H.B. Li, L.L.Chai, X.Q.Wang, X.Y. Wu, G.C.Xi, Y.K.Liu and Y.T Qian, *Cryst. Growth Des*. 2007, **7**, 1918-1922.

45. X. C. Jiang, Y. Xie, J. Lu, L. Y. Zhu, W. He and Y. T. Qian, *Adv.Mater.,* 2001, **13**, 1278–1281.

46. D.Venkappayya and D.H. Brown, *Indian J.Chem*., 1974, **12**, 838-839.

47. M. Nowsath Rifaya, T. Theivasanthi and M. Alagar, Nanoscience and Nanotechnology 2012, **2**, 134-138.

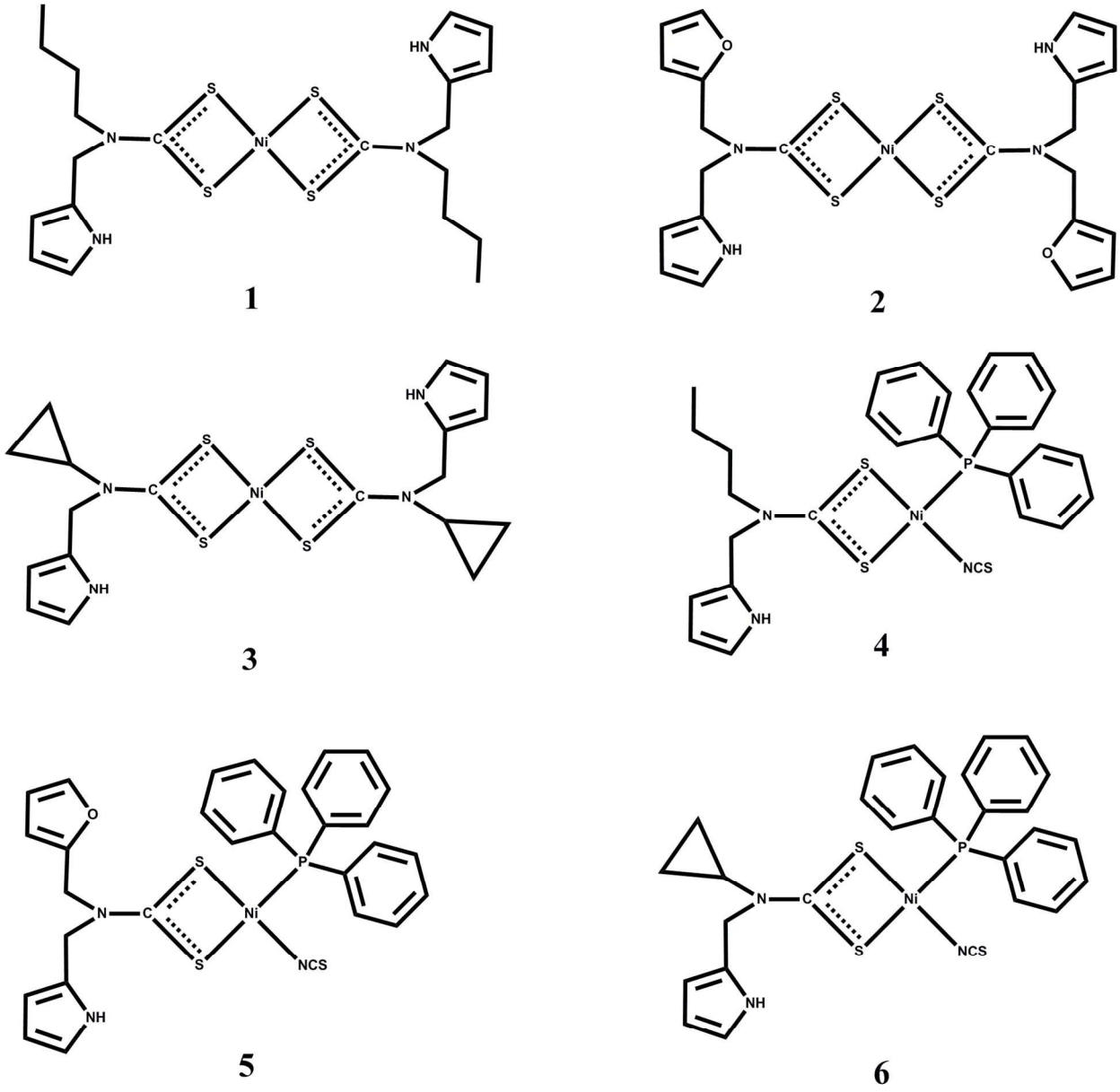

Scheme 1

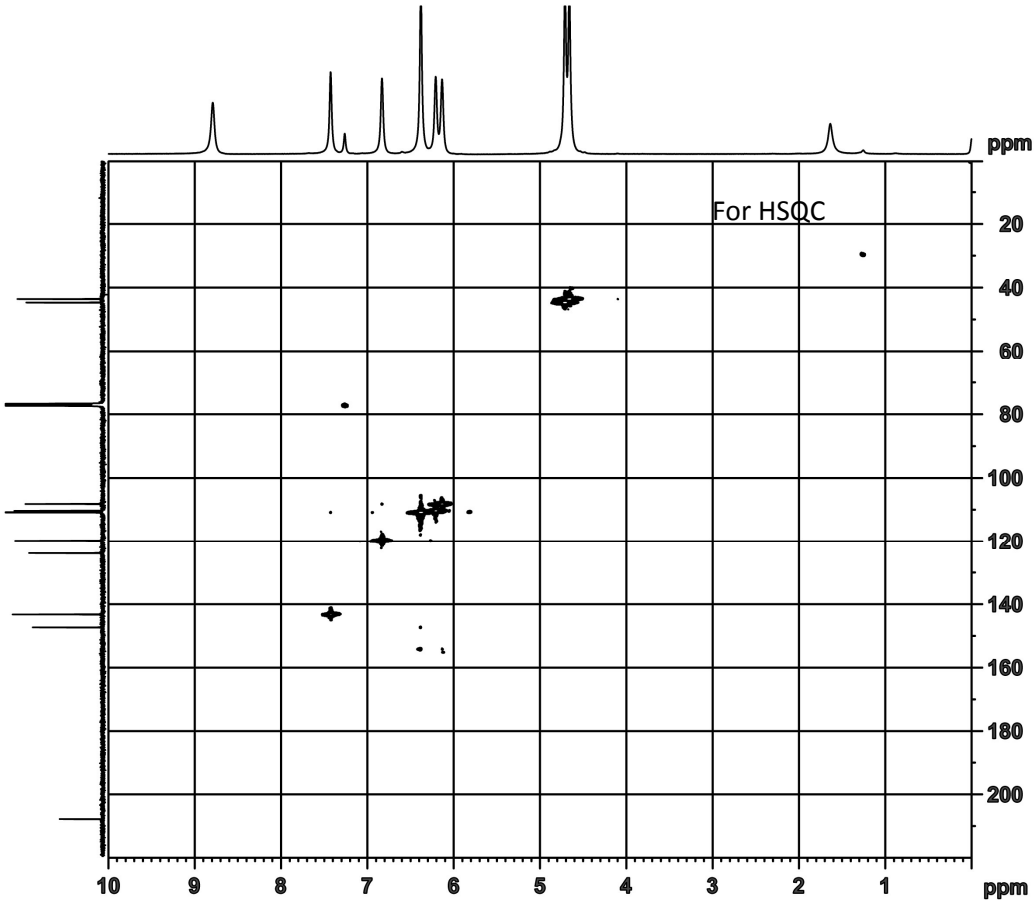

Fig. 1

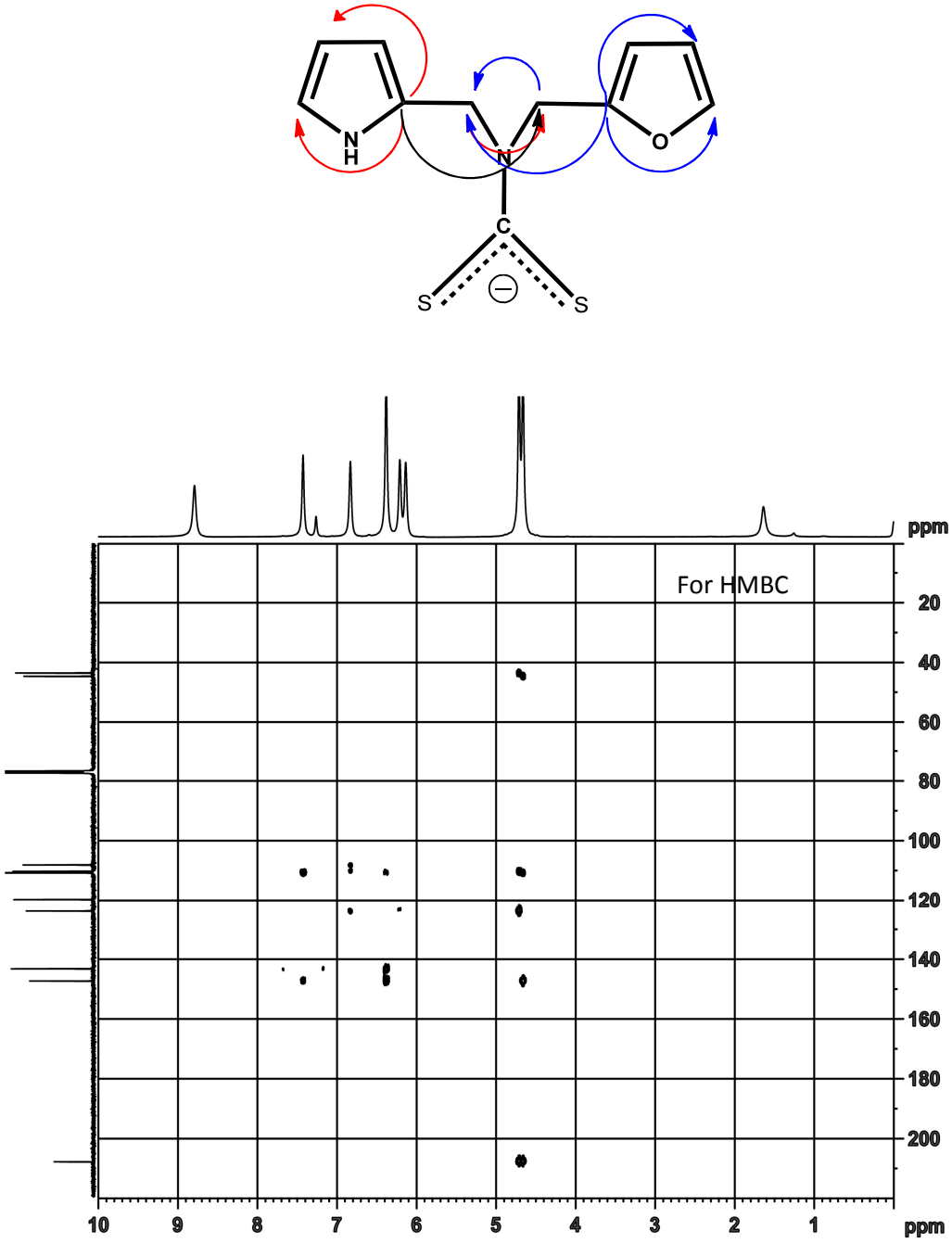

Fig. 2

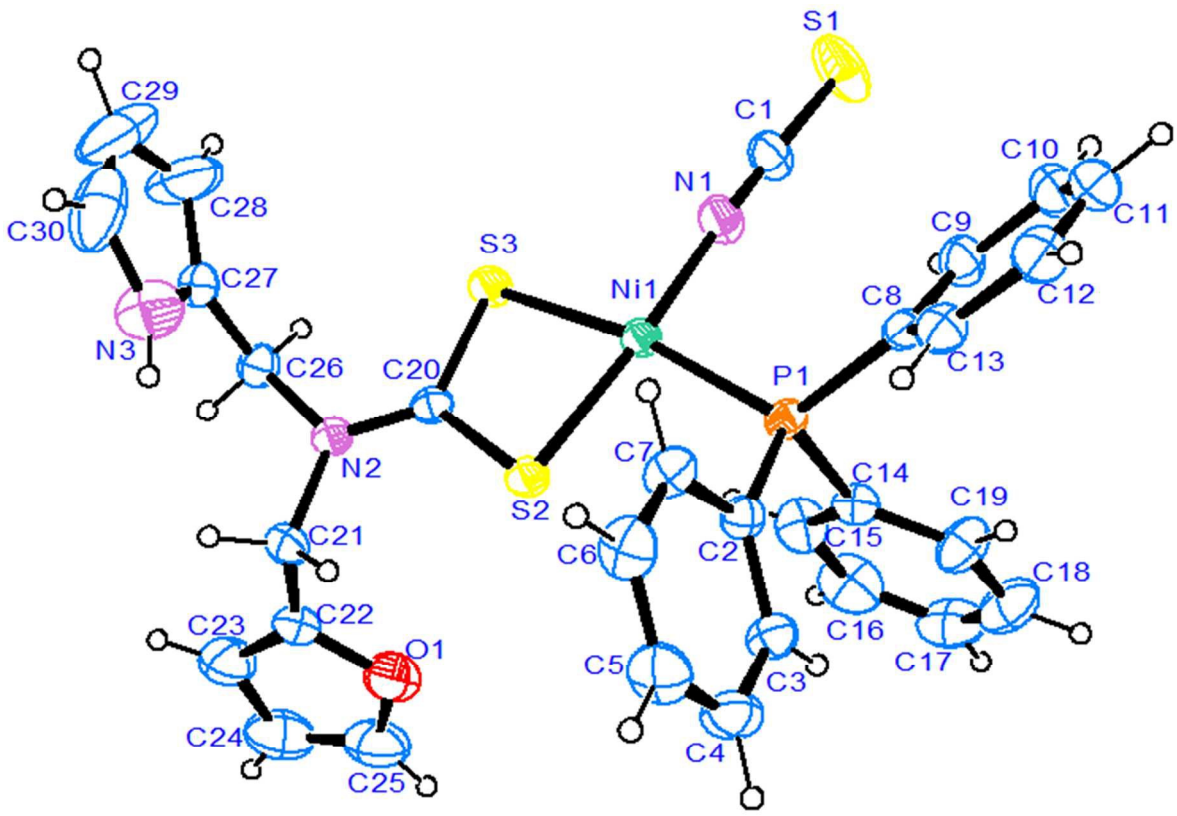

Fig. 3

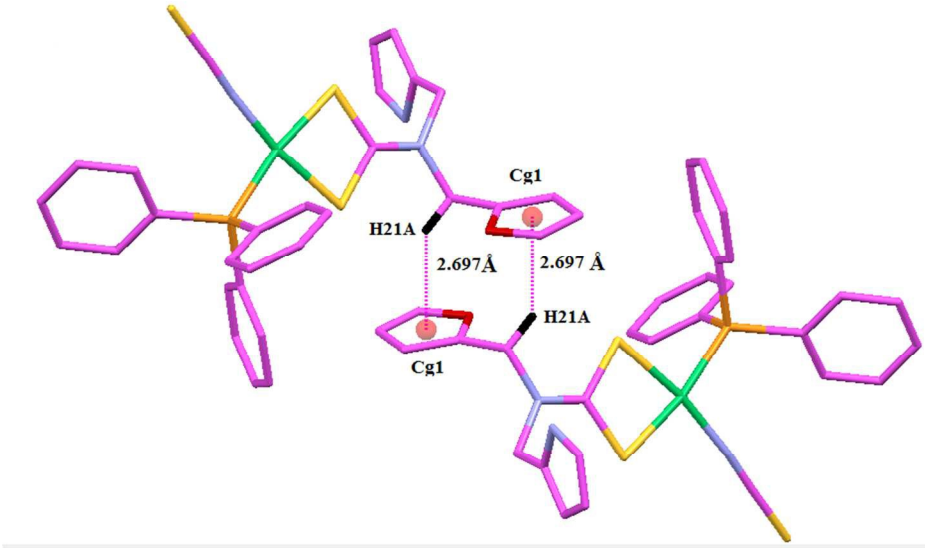

Fig. 4

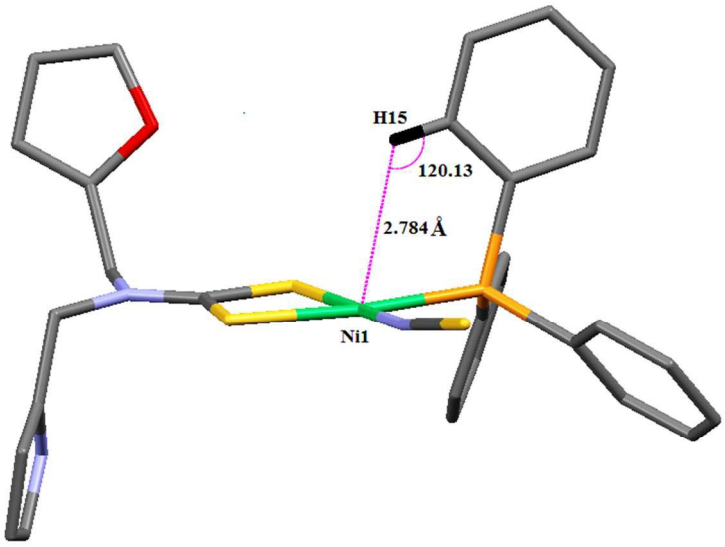

Fig. 5

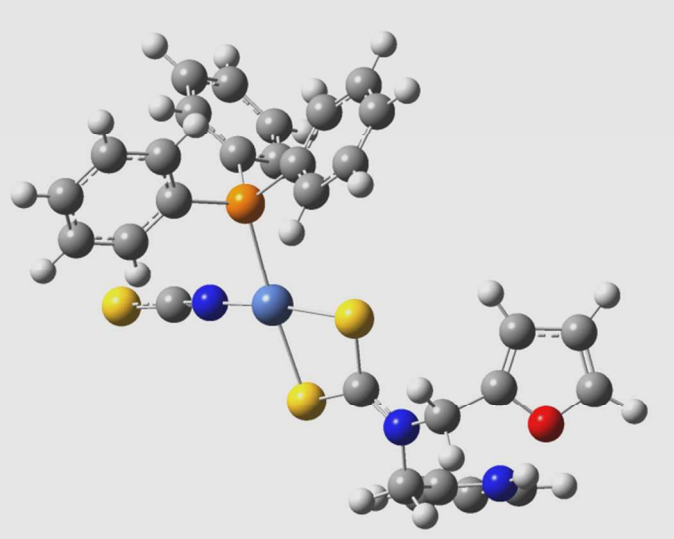

Fig. 6

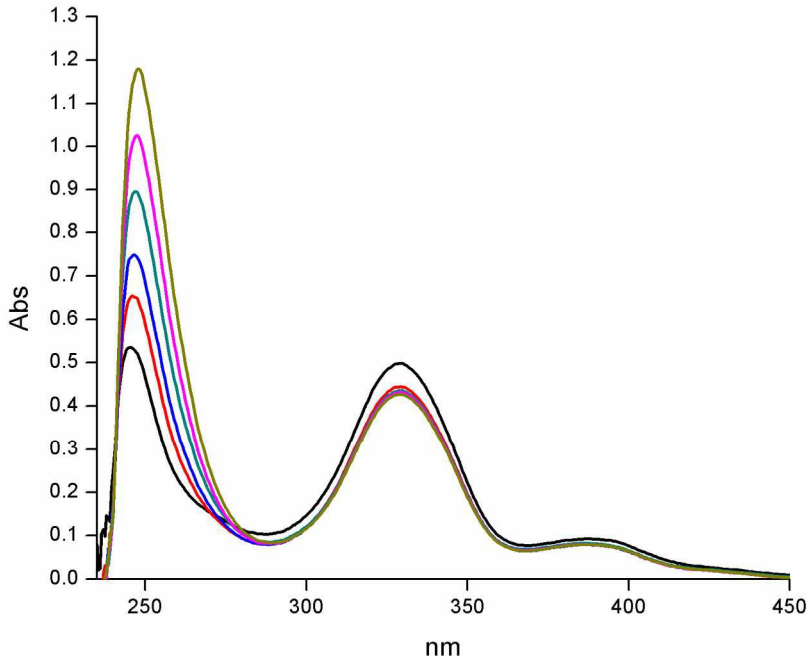

Fig. 7

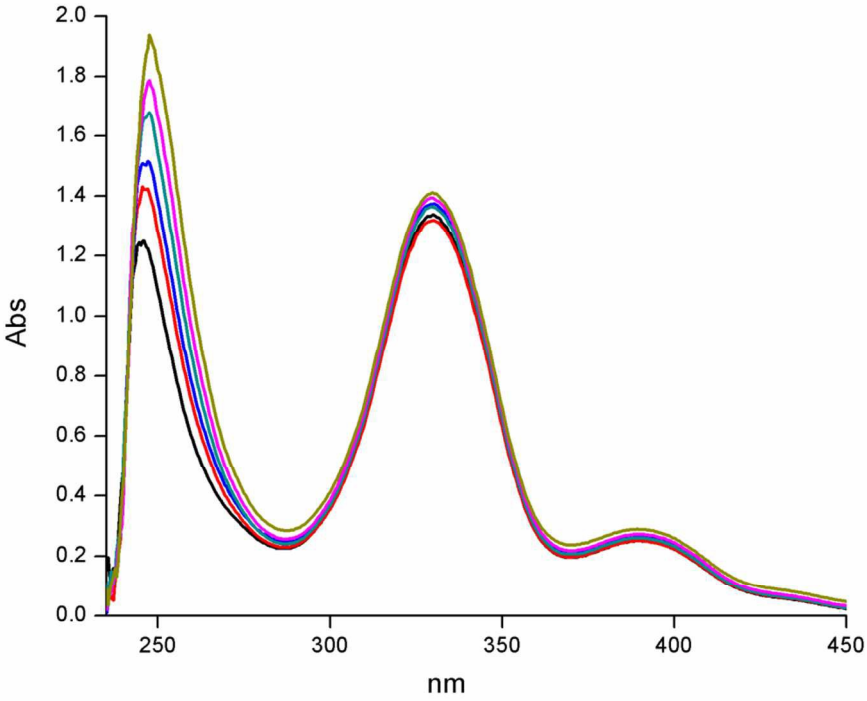

Fig. 8

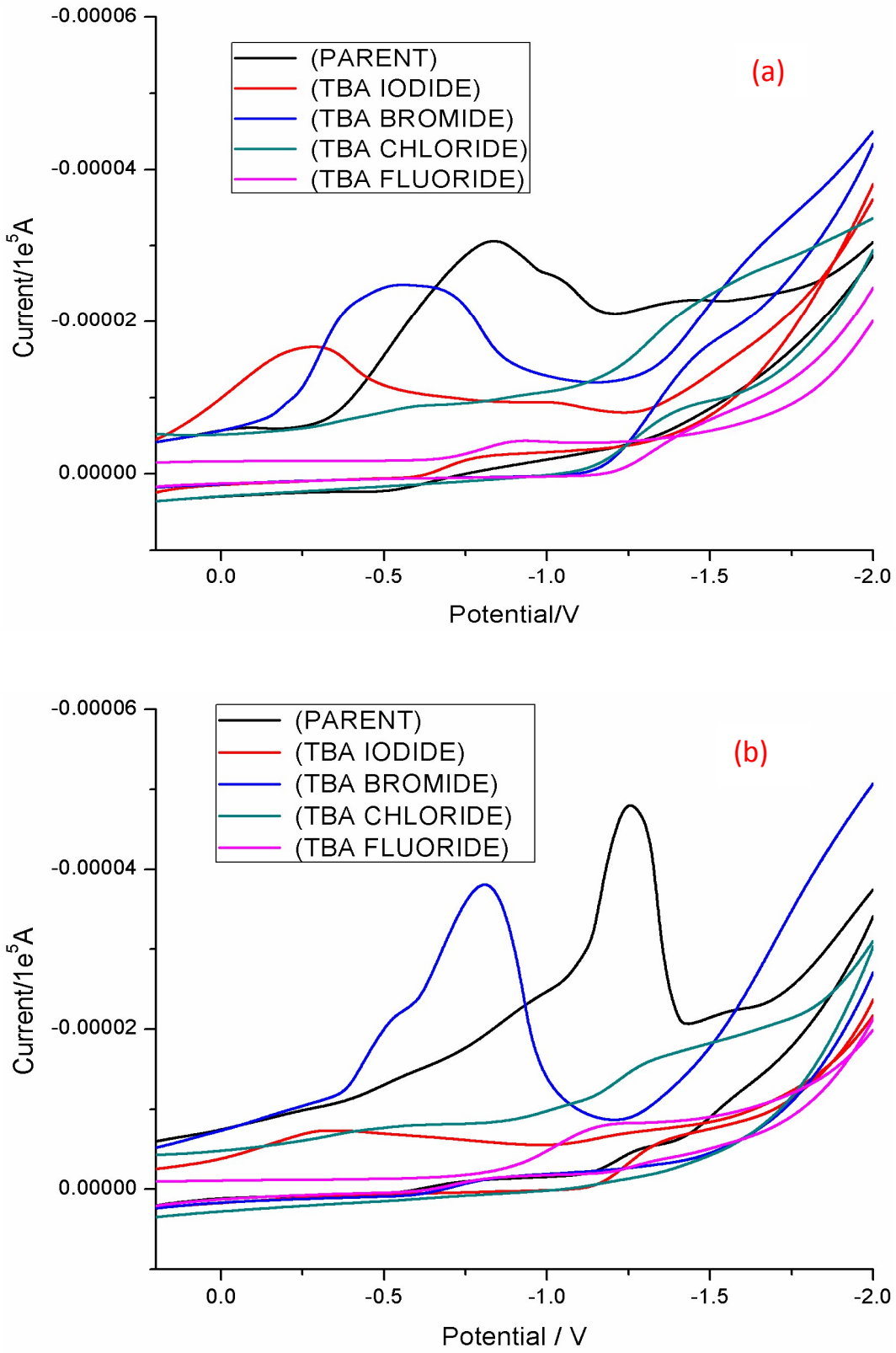

Fig. 9

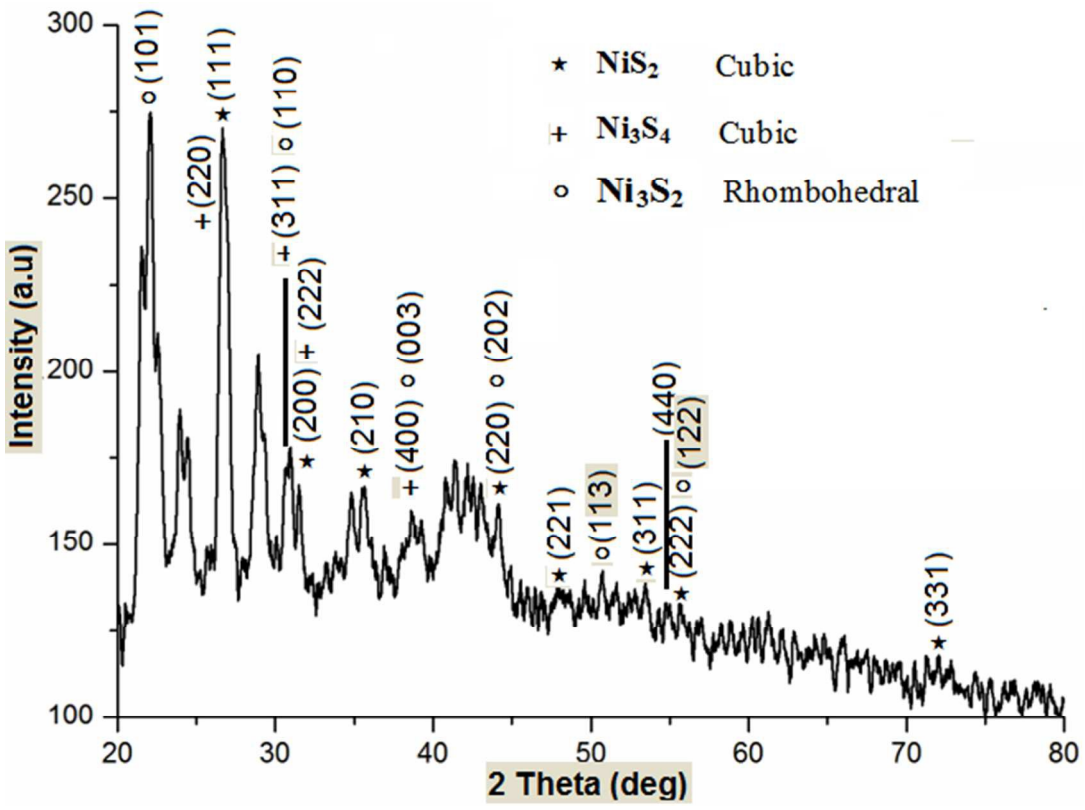

Fig.10

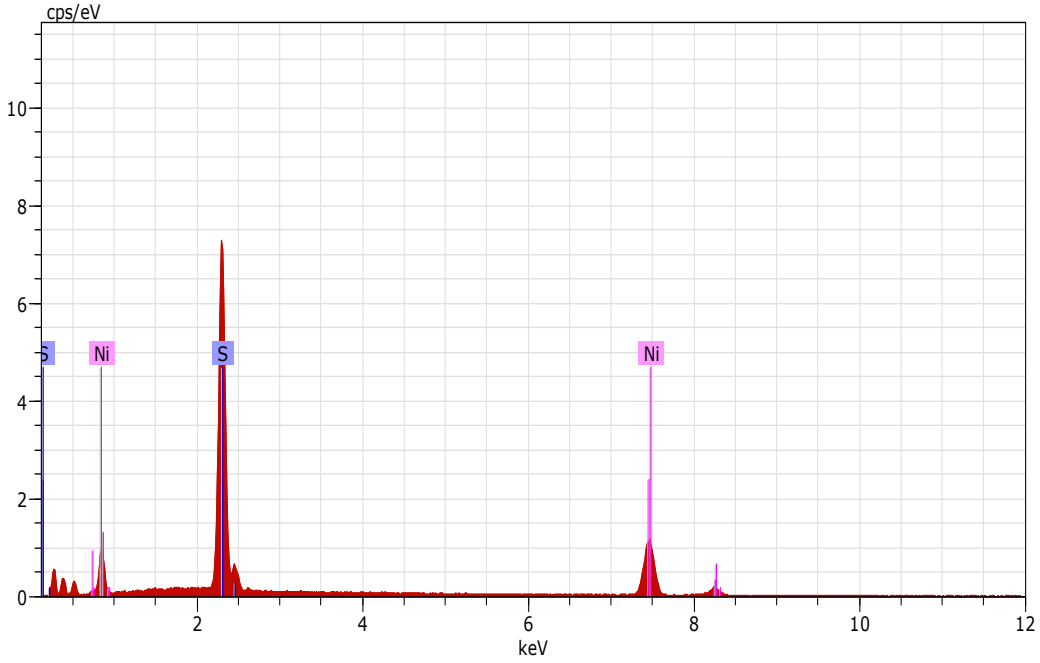

Fig. 11

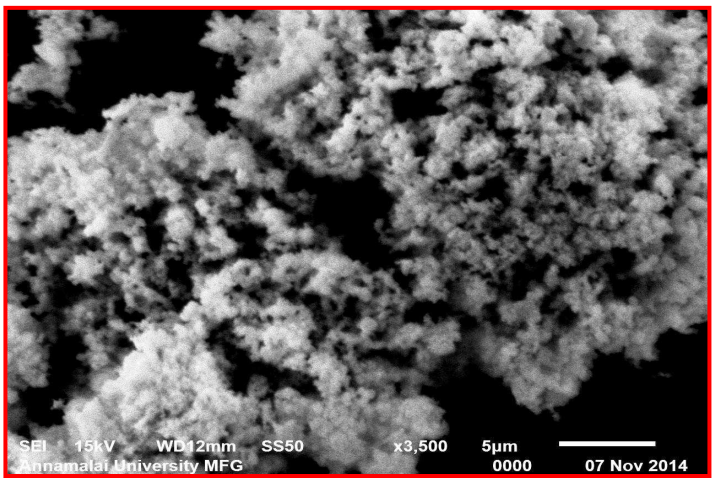

Fig. 12.

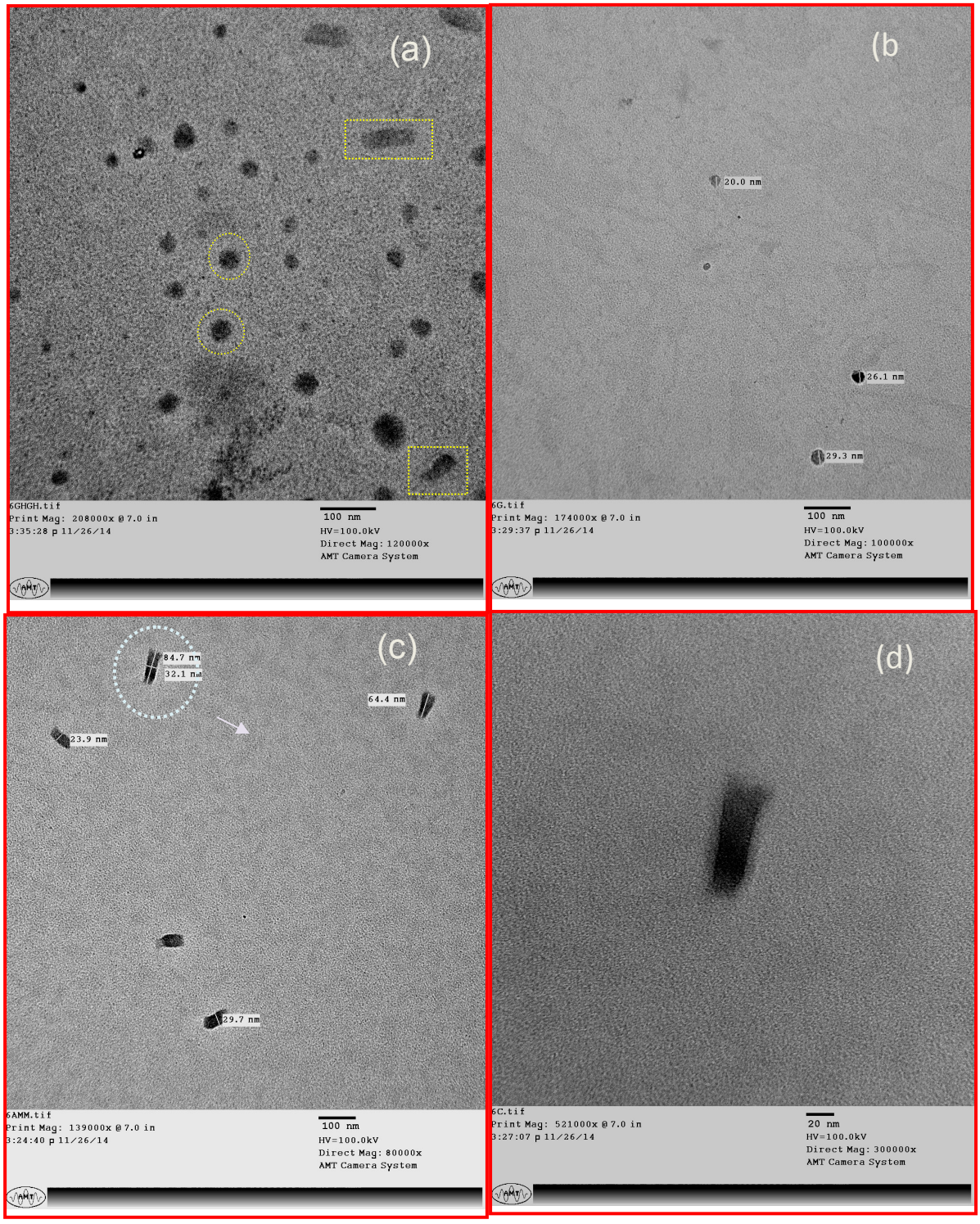

Fig. 13.

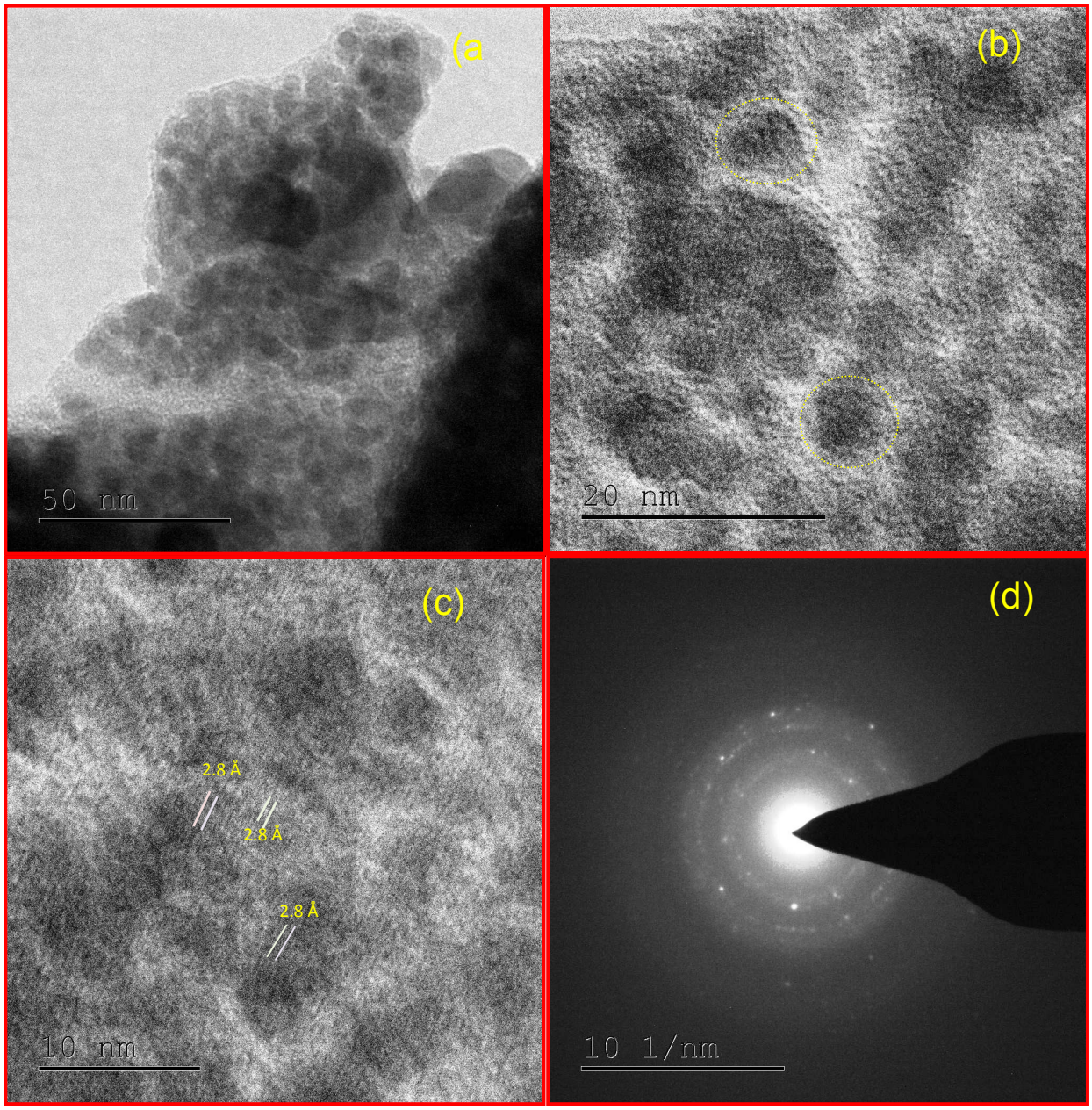

Fig. 14

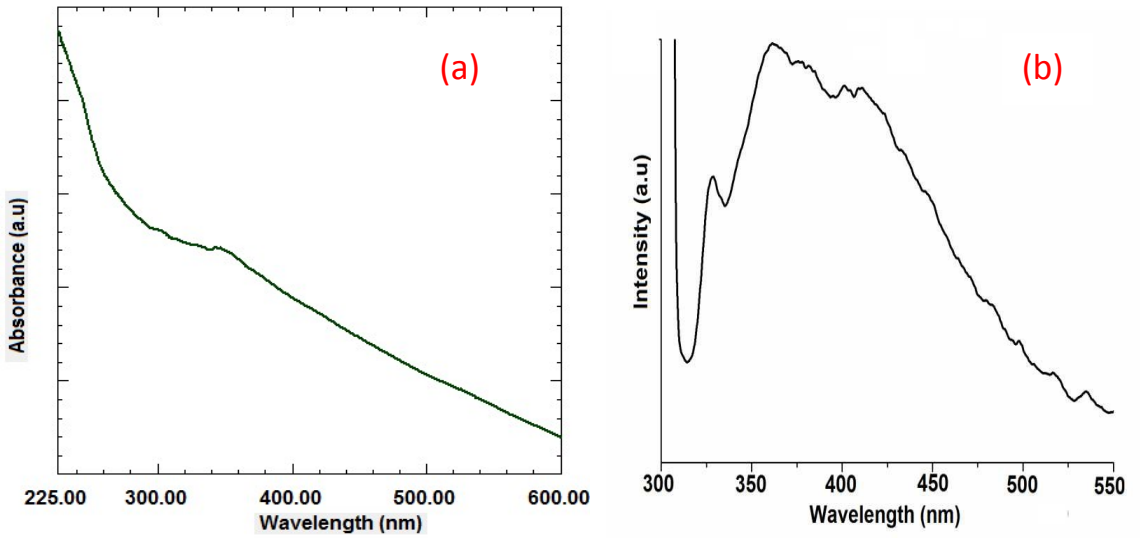

Fig. 15

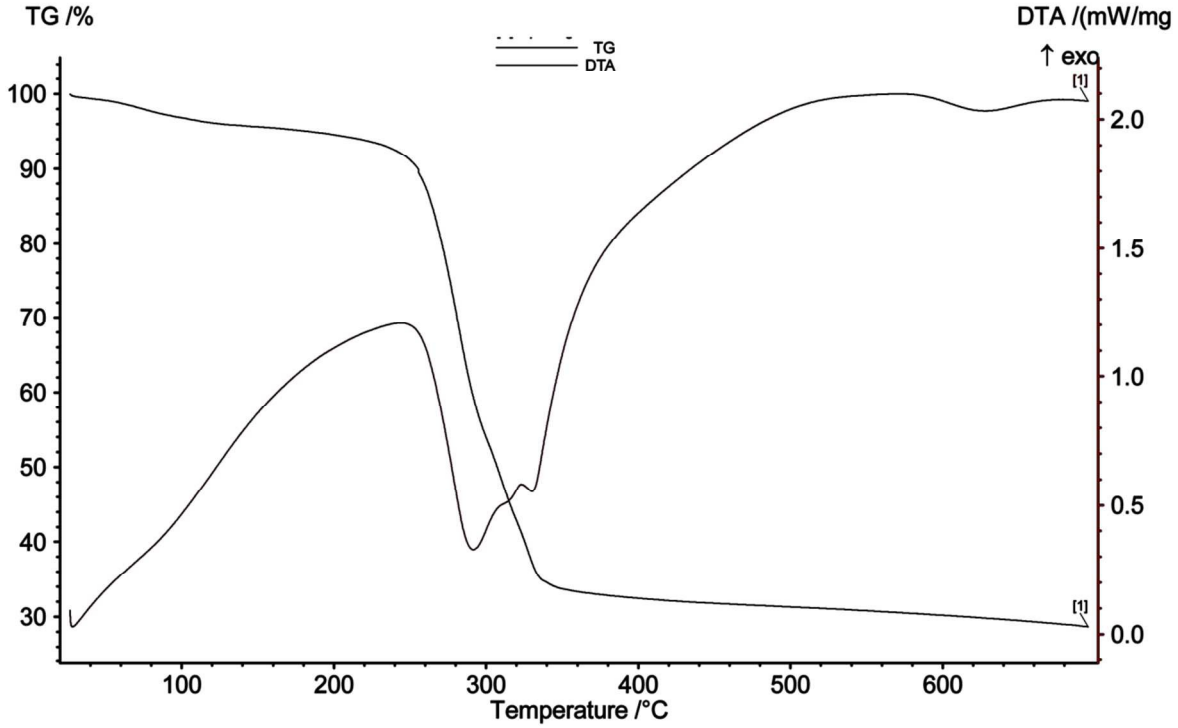

Fig. 16.

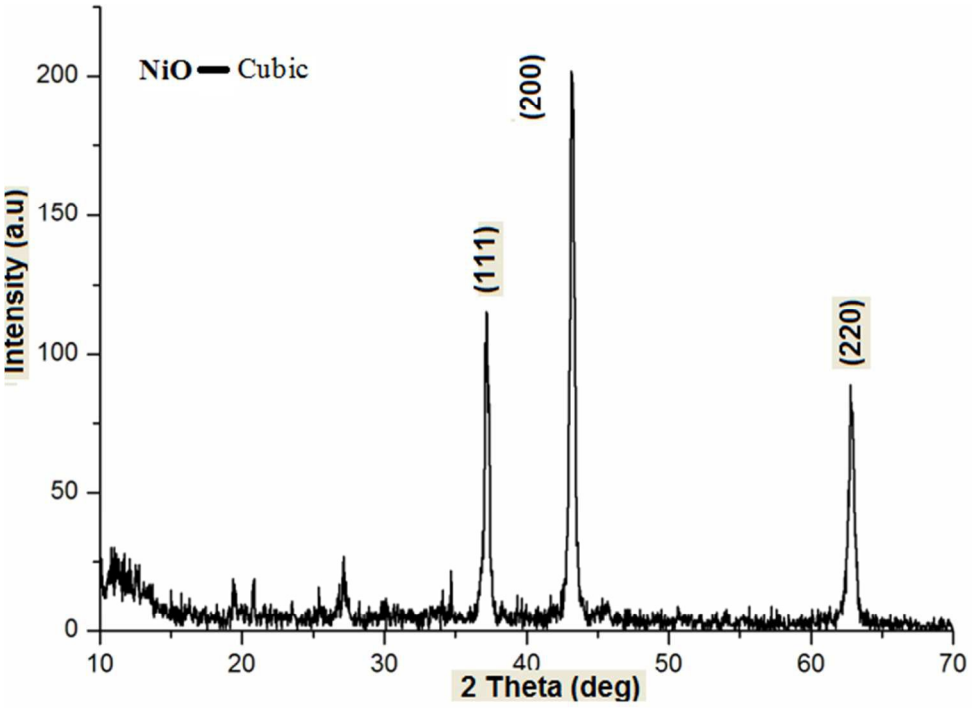

Fig. 17

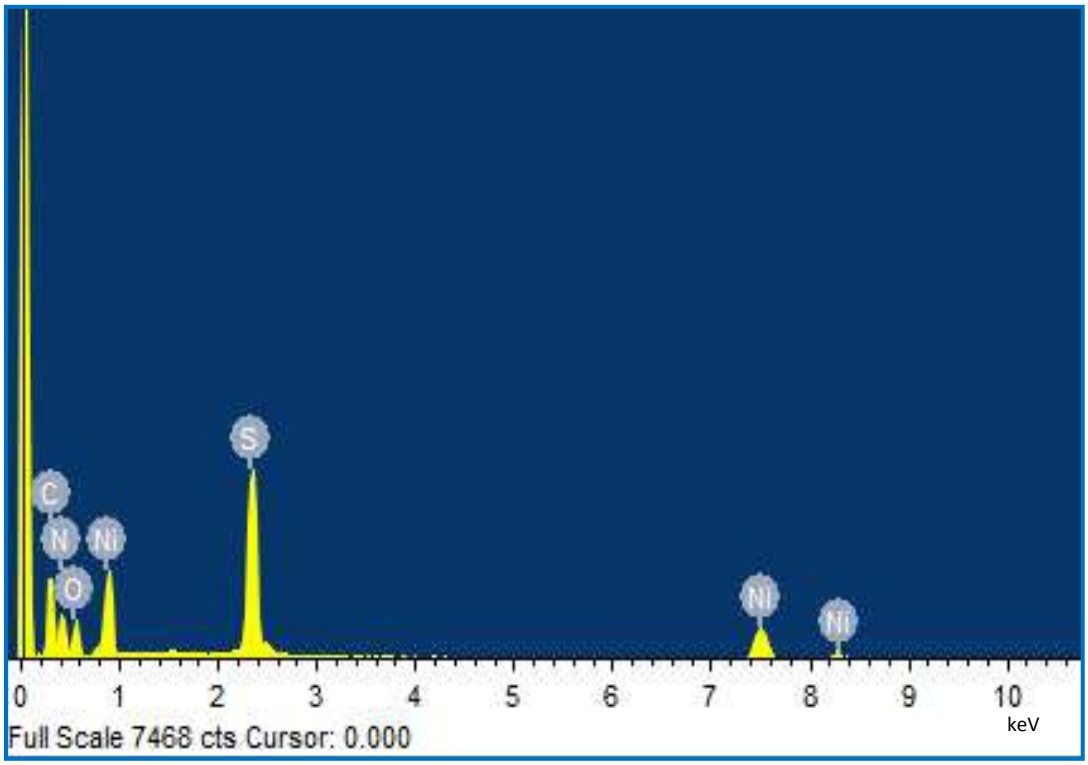

Fig. 18

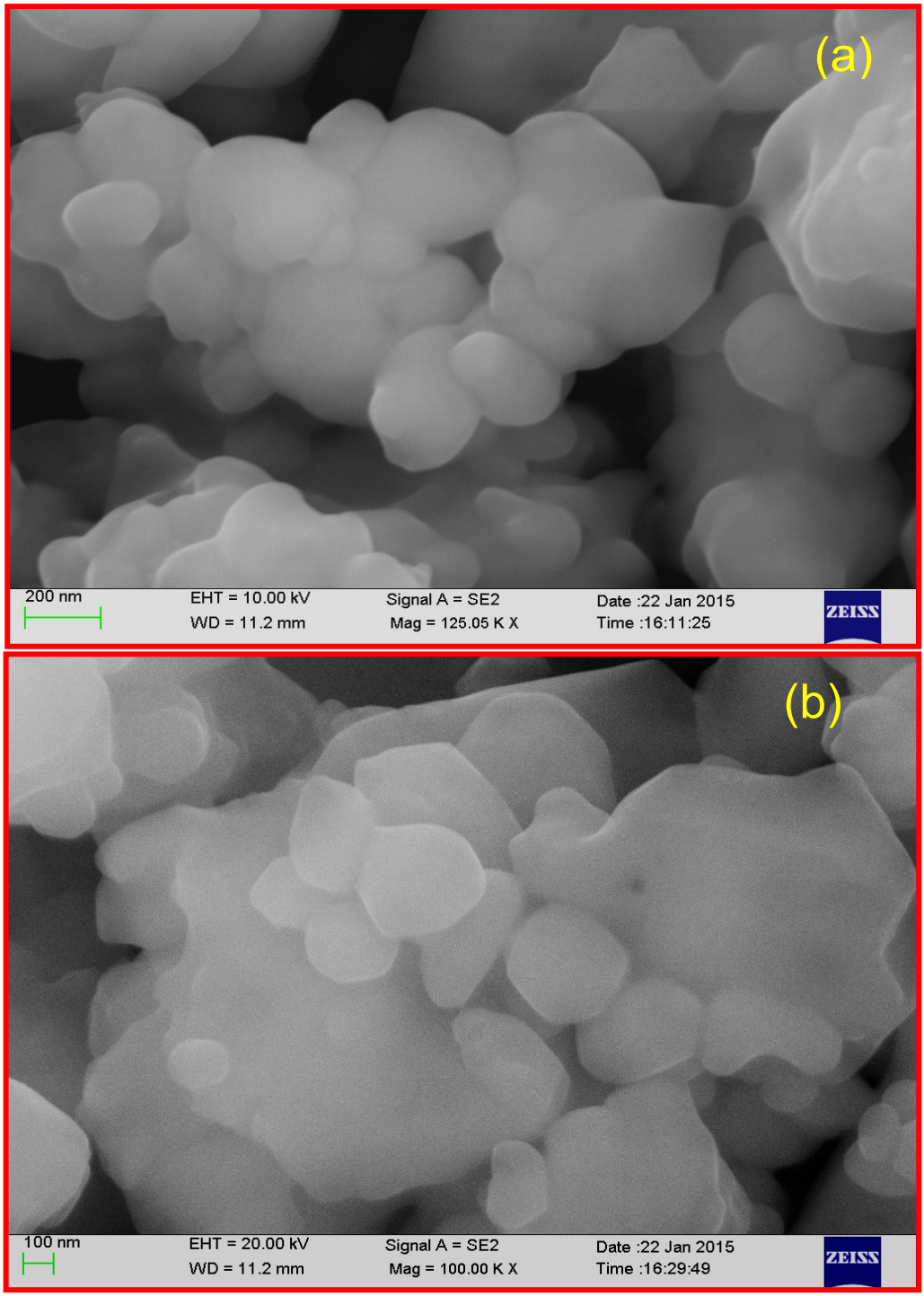

Fig. 19

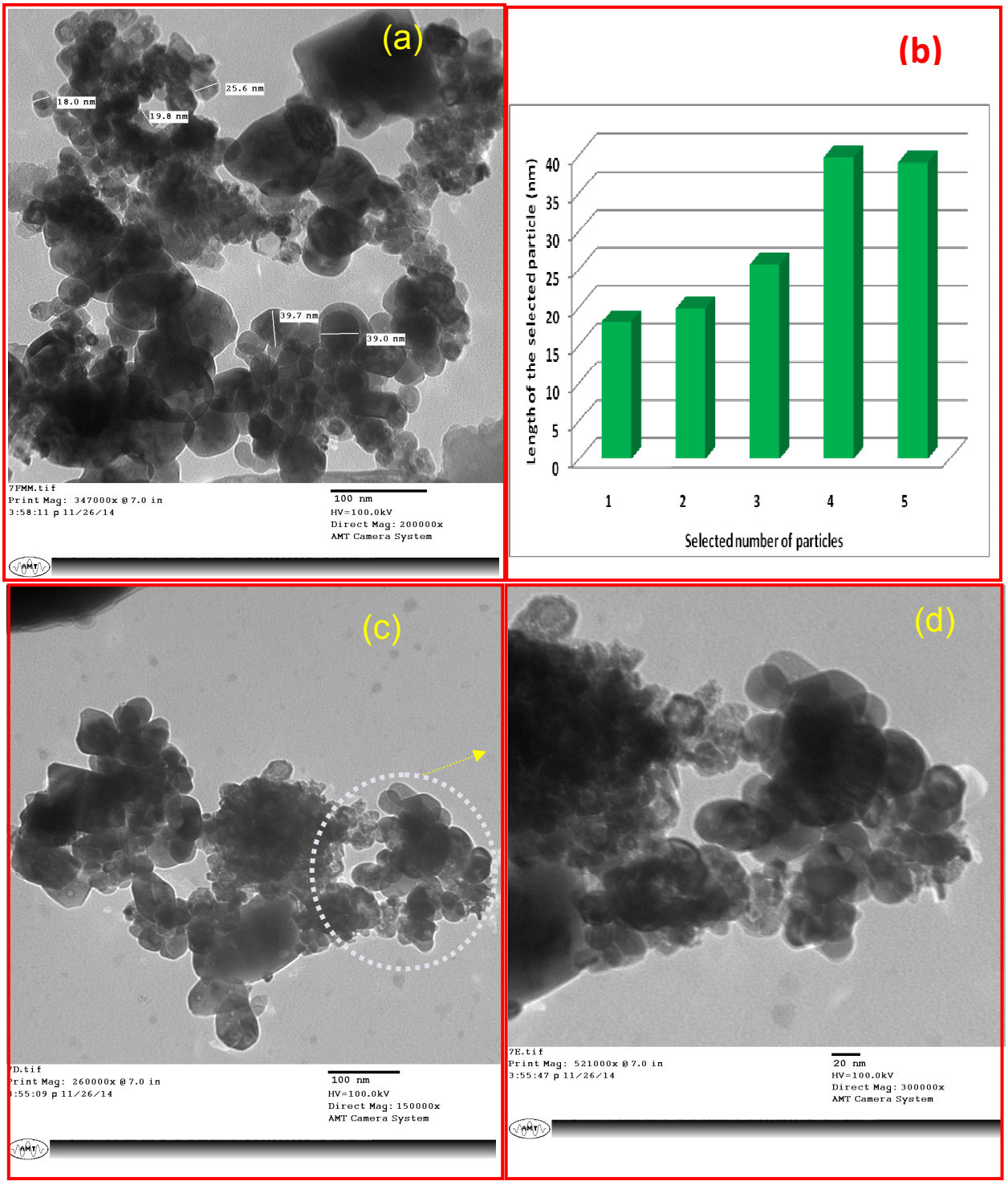

Fig. 20

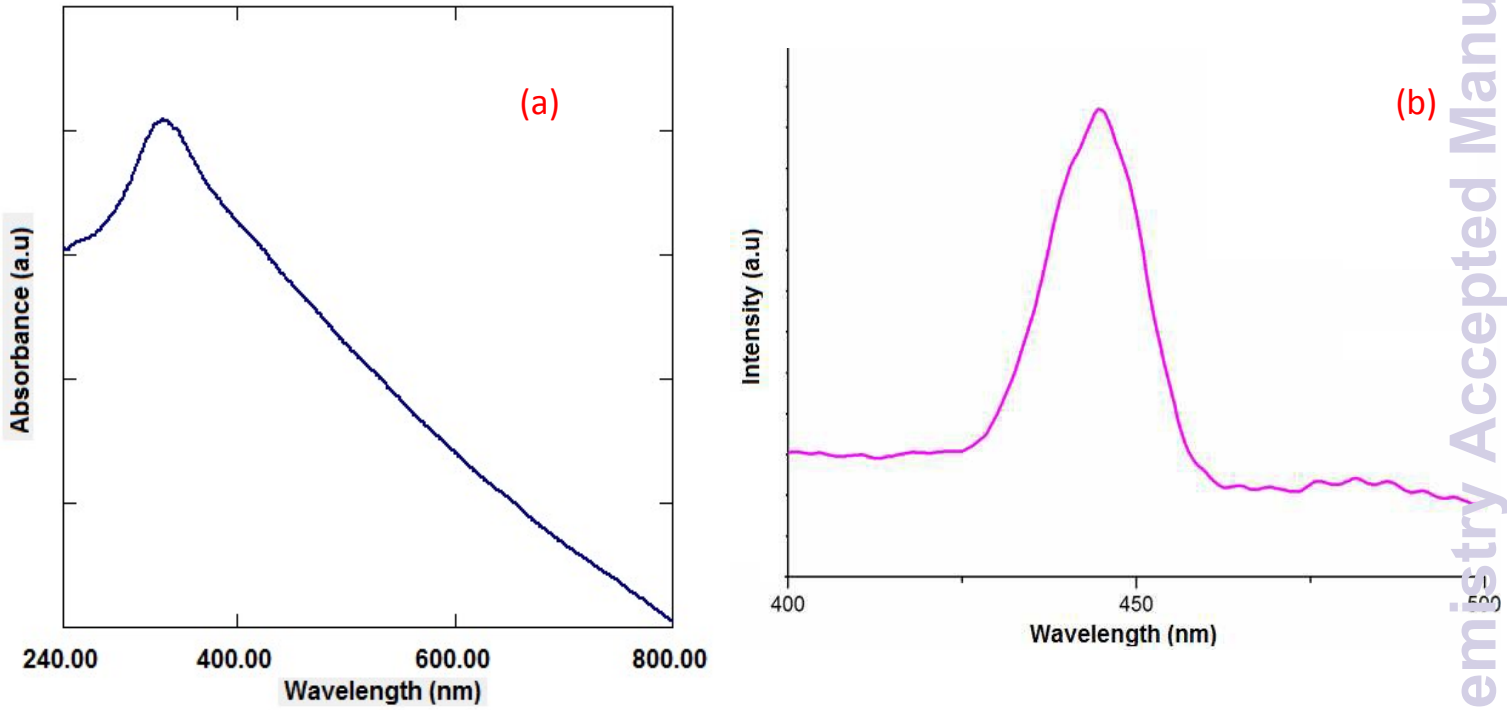

Fig.21